NTNU

Norwegian University of
Science and Technology

Cellular Uptake of Nanoparticles by Sonoporation

Sigurd Hanstad

Nanotechnology
Submission date: June 2017
Supervisor: Catharina de Lange Davies, IFY

Norwegian University of Science and Technology
Department of Physics

Preface

This thesis was carried out at the department of physics at NTNU during the spring of 2017, and marks the end of my five years as a student in Trondheim. It is also a continuation of my project thesis carried out during the fall of 2016. Parts of the two reports will therefore be somewhat similar in their theory and materials and methods parts.

I would like to thank Sofie Snipstad and Catharina de Lange Davies for always being available for help and support throughout the semester. Their knowledge and guidance has been absolutely necessary for the progression of this project. I would also like to thank Kristin Grenstad Sæterbø for training and support in cell culturing, and for always having answers to my questions. I would like to extend my sincerest thanks and appreciation to Astrid Bjørkøy for training and assistance in imaging cells, for hours of patience, but most of all for her help with analyzing images of the treated samples, and for writing the script that made this possible. I would also like to thank Anne Rein Hatletveit and Yrr Mørch for providing microbubbles and nanoparticles, and for helpful advice regarding the microbubbles throughout the semester. To Ragni, thank you for proofreading all of this, and for keeping my spirits up during the last, longest and most intense days of my student life.

Finally, I would like to thank everyone who has been a part of my life here at NTNU for making these years so memorable, and for making it so hard to leave Trondheim. You will be missed.

Trondheim - June 11, 2017

Sigurd Hanstad

Abstract

Encapsulation of anti-cancer drugs in nanoparticles (NPs) can solve many of the problems and side-effects related to cancer treatment today. By exposing micrometer-sized gas-filled bubbles to ultrasound, cellular uptake of NPs can be enhanced through a mechanism called sonoporation, or through enhanced endocytosis by affected cells. Much research has been done on sonoporation, but in most cases using small-molecular uptake agents rather than NPs, in combination with lipid microbubbles (MBs).

In this project varying ultrasound parameters were applied to MBs stabilized by a shell of poly(isohexyl cyanoacrylate) (PIHCA) NPs in order to establish their dependency on factors such as mechanical index (MI), pulse repetition frequency (PRF) and cycle length. Additionally, commercially avaialble Sonazoid MBs were used in order to compare the two MBs in terms of their ability to enhance cellular uptake of NPs following ultrasound treatment.

A significantly increased uptake compared to untreated control cells was achieved following ultrasound treatment with NP-stabilized MBs. Cellular uptake was seen in two forms, termed simple and clustered uptake, involving low and very high amount of uptake, respectively. The cellular uptake of PIHCA NPs was found to depend on the pressure applied in that an MI of 0.2 or above was required to increase the uptake compared to the control. Above this MI, the uptake did not seem to increase with increasing MI. It is hypothesized that there exists a threshold below which the biophysical effect of the ultrasound treatment is too small for the NPs to enter the cells. Above this threshold however, the pores created by the sonoporation effect seems to be big enough for most NPs to enter. This threshold is believed to lie between 0.1 and 0.2 MI. Uptake was also seen at 4°C, indicating that enhanced endocytosis does not play an important role in the uptake of the NPs, and that sonoporation is the main uptake mechanism. Increasing the PRF lead to a significant increase in NPs embedded in cellular membranes. In spite of this, the cellular uptake was not increased, likely due to the composition of the MBs.

The use of commercial Sonazoid MBs lead to significantly lower uptake than when using the NP-stabilized MBs. This suggests that the presence of NPs at the MB shell is important, and that it is mainly the NPs of the shell that are taken up, and not free NPs in the solution.

Sammendrag

Innkapsling av kreftmedisiner i nanopartikler (NPs) kan løse mange av problemene og bivirkningene knyttet til kreftbehandling i dag. Ved å eksponere mikrometer-store gassfylte bobler for ultralyd, kan opptak av NP økes gjennom en mekanisme som kalles sonoporering, eller gjennom ultralyd-indusert endocytose av berørte celler. Mye forskning har blitt gjort på sonoporering, men i de fleste tilfeller ved bruk av småmolekylære stoffer snarere enn NPs, samt i kombinasjon med lipid-mikrobobler.

I dette prosjektet ble varierende ultralyd-parametre testet på mikrobobler (MBs) stabilisert av et skall av poly (isoheksyl cyanoakrylat) (PIHCA) NPs for å fastslå deres avhengighet av faktorer som mekanisk indeks (MI), pulsrepetisjonsfrekvens (PRF) og sykluslengde. I tillegg ble kommersielle Sonazoid MBs brukt for å sammenligne de to MBs med hensyn til deres evne til å øke opptak av NPs i celler etter ultralydbehandling.

Et signifikant økt opptak sammenlignet med ubehandlede kontrollceller ble oppnådd etter ultralydbehandling med NP-stabiliserte MBs. Opptak i celler ble sett i to former, betegnet enkelt og klynget opptak, med henholdsvis lavt og svært høyt opptak. Opptaket av PIHCA NPs ble funnet å avhenge av påført trykk ved at en MI på 0.2 eller høyere var nødvendig for å øke opptaket sammenlignet med kontrollceller. Over denne MIen syntes opptaket ikke å øke med økende MI. Det blir foreslått at det over en MI-terskel dannes store nok porer av sonoporeringen til at de fleste NPs kommer inn. Denne terskelen antas ligge mellom 0.1 og 0.2 MI. Opptak ble også sett på 4°C, noe som indikerer at ultralyd-indusert endocytose ikke spiller en viktig rolle i opptaket av NPs, og at sonoporering er hovedopptaksmekanismen. Økning av PRF fører til en økning i NPs kolokalisert med cellemembraner. Til tross for dette ble opptaket av NPs ikke økt, sannsynligvis på grunn av sammensetningen av MBs.

Bruken av kommersielle Sonazoid MBs fører til betydelig lavere opptak enn ved bruk av NP-stabiliserte MBs. dette antyder at tilstedeværelsen av NPs på MB-skallet er viktig, og at det hovedsakelig er NPs på skallet som er tatt opp, og ikke frie NPs i løsningen.

Contents

Preface i

Abstract iii

Sammendrag v

Contents

1 Introduction 1

2 Theory 3
2.1 Cancer . . . 3
2.2 The EPR effect . . . 4
2.3 Nanoparticles as drug carriers . . . 4
2.4 Barriers to drug delivery . . . 6
2.5 Cellular uptake of nanoparticles . . . 7
2.6 Ultrasound . . . 9
2.6.1 Microbubbles . . . 12
2.7 Effects of ultrasound on tissue and microbubbles . . . 13
2.7.1 Thermal effects . . . 14
2.7.2 Non-thermal effects . . . 14
2.7.3 Acoustic cavitation . . . 15
2.8 Sonoporation . . . 16
2.9 Confocal laser scanning microscopy . . . 17

3 Materials and Methods 21
3.1 Cell cultivation . . . 21
3.2 Seeding of cells in CLINIcell . . . 21
3.3 Experimental setup . . . 22
3.4 Experiment preparations and ultrasound treatment . . . 23
3.5 Microbubbles and nanoparticles . . . 25
3.6 Staining . . . 26
3.7 Co-incubation of Sonazoid microbubbles and free nanoparticles . . . 26
3.8 Qualitative inspection of uptake . . . 27
3.9 Quantitative inspection of uptake . . . 28

4 Results 31
4.1 Uptake of PIHCA NP/MBs . . . 31
4.1.1 Qualitative inspection of uptake . . . 31
4.1.2 Control sample . . . 32
4.1.3 Quantitative inspection of uptake . . . 35
4.2 Uptake of NPs after co-incubation . . . 42

5 Discussion **47**
5.1 Cellular uptake of NPs after ultrasound treatment 47
5.2 Confluency of cell layer in CLINIcell during treatment 52
5.3 Effect of cycle length and PRF on cellular uptake 53
5.4 Co-incubation of free NPs and MBs 56
5.5 Future work and clinical applications 57

6 Conclusion **61**

References **63**

1 Introduction

According to the 2014 World Cancer Report published by the International Agency for Research on Cancer, a division of the World Health Organization, 14 million people were diagnosed with cancer and 8.2 million died from it in 2012. By 2025, the number of new annual cancer cases is expected to exceed 20 million. The number of annual deaths resulting from cancer is expected to exceed 20 million within the next twenty years. The increase in new cancer cases is partially due to better diagnostics, but also because of an increasingly unhealthy way of life with respect to pollution, diet, etc. [1].

The treatment for cancer is a terrible strain, both mentally, physically and economically, on patient, relatives and society. Because of this, finding a cure for cancer has in many ways been regarded as the holy grail of medical science. Even though there is a long way to go until we get a safe and reliable cure for cancer, many big steps are taken in the right direction every year, and many innovative and promising solutions are on the way.

The most common ways to treat cancer today are surgical removal of the tumor, radiation therapy, and chemotherapy, often in combination. Treatment depends on the type and location of the cancer, but often involves chemotherapy. Chemotherapy is in many cases a gift to cancer patients, and many of them are cured and go on to live long lives. This treatment is however a double-edged sword. On one hand, it could cure the cancer, but on the other hand, it might lead to severe side-effects. The biggest flaw with chemotherapy is its lack of specificity, which means that more than just the cancer is attacked by the anti-cancer agents. As this agent is designed to kill cells, a lack of specificty means that healthy cells are also killed by it. Hair cells being attacked by the anti-cancer drug is why many cancer patients lose their hair during treatment, but the side effects do not stop there. Nausea, deteriorating nails, weakened immune system and damage to inner organs, are just some of the side effects that might arise from chemotherapy [2, 3].

One solution to these side effects is to encapsulate the anti-cancer drugs in nanoparticles, which would shield the medicine from the body - and vice versa - until it reaches the desired location [3, 4, 5]. These nanoparticles can in theory be tailored to each patients specific need, allowing for targeting of the tumor cells, and effective and safe treatment. However, even if these nanoparticles carrying anti-cancer drugs reach the cancer cells, there is no guarantee that they will be taken up efficiently by the cells, which is a requirement for this approach to be clinically usable. To solve this issue, researchers have applied ultrasound as a tool to enhance cellular uptake.

The use of ultrasound, when applied to microsized gas bubbles, can lead to biophysical effects in the tissue surrounding the bubbles. One such effect is sonoporation, the formation of small pores in nearby cell membranes, through which nanoparticles can enter the cell. Another possible effect is enhanced endocytosis by the affected cells. Both of these mechanisms can enhance uptake of nanoparticles, and potentially make nanoparticles a viable option as a drug carrier for cancer treatment. The combination of ultrasound with microbubbles

to elicit a biophysical response is the subject of this thesis. Although the technique has been around for some time, much of it is poorly understood, and the conditions for successful sonoporation varies with each type of microbubble and nanoparticle used.

Many different types of microbubbles and uptake agents have been attempted for successful sonoporation, with varying degrees of success. Most studies so far have used co-incubation of microbubbles alongside free nanoparticles. In this thesis, however, a new type of microbubble, stabilized by a shell of nanoparticles is used [6]. The goal of this design is to have NPs close enough to the pore opening during sonoporation for them to enter the cell before the pore closes.

This thesis is a continuation of a project thesis written and submitted during the fall of 2016. In that project, sonoporation was attempted using the same bubbles and particles as in this project. Towards the end of the project, cellular uptake of nanoparticles was seen. One of the goals in this present thesis is to once again establish successful sonoporation, and hopefully gain valuable insight into the mechanisms behind it.

2 Theory

2.1 Cancer

The intracellular cascades of reactions and mechanisms taking place in our cells at all times, involved in cell divison, maintenance, or other cell functions, are immensly complex, and errors do occur. In most cases the body kills defective cells before they can do any harm. Sometimes, however, these cells slip past the security mechanisms. Such errors can for instance be realted to cell growth and death. In healthy cells, there is a finely tuned balance between cell growth and death. If this balance is off, cells can begin to grow uncontrollably. The fault often lies in a cell's built-in control which ensures that defective or excess cells undergo apoptosis, a controlled form of cell death. When these "suicide" mechanisms fail, the cells are allowed to accumulate in the tissue. This accumulation eventually leads to the formation of what is known as a tumor. Uncontrolled, and often rapid, growth of defective cells is one of the hallmarks of cancer [2].

Almost any organ in our body can develop cancer, including the lungs, liver, breasts and prostate, but a tumor in itself is not necessarily deadly. The uncontrolled growth of cells, is not primarily what makes cancer such a dangerous condition. If the tumor cells are limited to just the primary tumor, and this tumor is situated in such a way that it can be surgically removed, the chances of survival can be good. Moles showing early signs of skin cancer can be cut away, and breast cancer is often treated by surgical removal of one or both breasts. Such a tumor is termed benign. The other class of tumors is termed malignant, which is a far worse diagnosis. This means that the cancer cells have spread from the primary tumor, through the blood, to other parts of the body. If this is the case, removal of the primary tumor might not cure the patient. Spreading of the cancer, metastasis, is another characteristic of cancer, and it is by far the most dangerous. Roughly 90 % of all cancer deaths are caused by the cancer spreading, rather than by the primary tumor itself [2].

Cancer is a terrible disease, both for the patients and their relatives, and it is a huge strain to society, both economically and in terms of resources. Considering the number of people affected at any given time, it is easy to understand why curing cancer is such a highly sought-after goal. Existing treatments are improving, and new chemotherapy drugs make the treatments better and the side-effects easier to live with. The most common ways to treat cancer today are surgical removal, radiation therapy, and chemotherapy - often the three are combined and the treatment tailored to each patient. None of them are without limitations, however. Surgical removal will not suffice if the cancer has spread or if it is located in a position in the body which makes surgery impossible. Radiation therapy on the other hand is a great strain on the patient's body, and although effective at killing cells, it is not cancer cell specific. The lack of specificity is also true for chemotherapy, yet it is still the treatment of choice in many cases [2].

Chemotherapy has saved many lives over the years, and is indeed a possible route back to health for many people. However, because of its lack of specificity,

the chemotherapy causes damage to the entire body. Loss of hair and nausea are well-known side-effects of chemotherapy, but the list is long, and includes side-effects such as a weakened immune system, infertility, impotence and a risk of serious complications to brain and nervous system, to name a few. These side-effects, and the strength of the poison itself, put strict limits on the doses and frequency of chemotherapy a patient can receive. Really high doses can even be lethal. Furthermore, there is no guarantee of the effectiveness of the treatment, as each and every cancer case is unique, and a given tumor might not respond to the given treatment. In short, cancer treatment has come a long way, but there is still much to be done. Although a definitive cure might still be considered science fiction, great strides are being made in laboratories around the world, including exciting approaches such as immunotherapy, hormone therapy, bone marrow transplantation, and sonoporation, which is the topic of this project [7, 8].

2.2 The EPR effect

When cells accumulate in tissue, they form a tumor. For this tumor to grow, the cells need nutrients, which are delivered through the blood. For the tumor to support its own abnormal growth, the tumor cells will signal for new blood vessels to form, a process called angiogenesis. However, because the tumor growth is often quite rapid, the angiogenesis happens too fast for the new blood vessels to form proper endothelial walls. The results are leaky blood vessels, with irregular gaps between the endothelial cells making up the blood vessel walls. This leaking can be exploited and used against the tumor, as will be described shortly. The body's lymphatic system is responsible for waste removal from tissue. In tumors, this lymphatic system is often malfunctioning. The result is an accumulation of fluids and waste in the tumor tissue. This is both good and bad from a drug delivery perspective: On one hand, it allows for drugs to stay longer in the tumor. On the other hand, this accumulation of liquids lead to a high pressure in the tumor, which makes extravasation from the blood vessels and into the tumor more difficult. The combined effect of these leaky vessels and the weakened clearance system is termed the enhanced permeability and retention (EPR) effect. First described by Matsumura and Maeda in 1986 [9], this concept has been widely exploited for drug delivery to tumors, as a kind of passive targeting mechanism. However, the degree of the EPR effect is heterogenous between tumors and even within a tumor, which leads to varying effectiveness of this approach. Other factors also influence the result. In fact, the uptake of nanoparticles in tumors is affected both by vascular density, collagen density and the interstitial pressure [10, 11].

2.3 Nanoparticles as drug carriers

Many new and innovative solutions for drug delivery are being developed. One approach involves nanoparticles (NPs) as drug carriers. As mentioned above, chemotherapy is one of the most common treatments for cancer patients today,

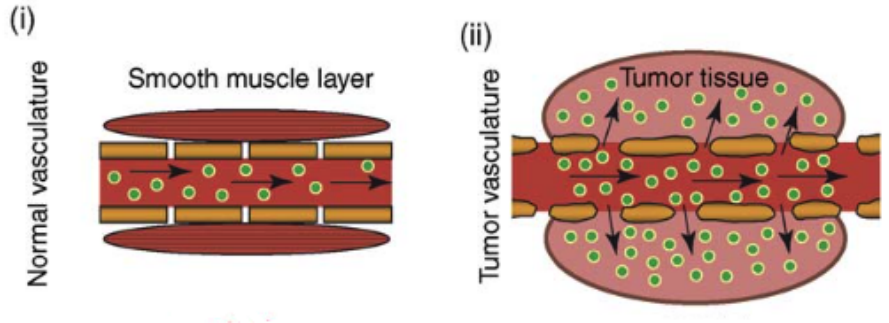

Figure 1: Demonstration of the EPR effect. (i) shows a normal vasculature, in which the endothelial cells making up the blood vessel wall are so tightly packed that the NPs do not escape. In (ii), a tumor vasculature is shown, with its characteristic leaky blood vessels. The NPs accumulate in the tumor tissue. Adapted from [11].

but due to its lack of specificity it comes with strict limitations on dosage and frequency of administration. By delivering the drugs capsuled in a protective NP, many of the drawbacks related to todays chemotherapy could potentially be solved. From a cancer treatment perspective, the goal would be a NP that carries a high amount of anti-cancer drugs, and that will actively and/or passively seek out only cancer cells before releasing its contents, effectively removing the cancer, leaving the rest of the body unharmed. These NPs could also increase circulation time in the body compared to free drugs, to ensure steady and high accumulation of drugs in the tumor, and could even be tailored to fit the needs of each individual patient.

The term nanoparticles is rather vague and in this context includes a wide range of drug carriers. In short, any nanosized material that can carry one or multiple drugs can be called a nanocarrier. These include liposomes, nanoshells, dendrimers, polymeric NPs, carbon nanotubes and micelles, to name a few [12]. Of these, polymeric NPs have emerged as promising drug carriers due to advantages such as easy fabrication and functionalization, biocompatibility, sustained drug release and controllable degradation rate [13]. One family of such polymeric NPs is the poly(alkyl cyanoacrylate) (PACA) NPs, one of which (poly(isohexyl cyanoacrylate) (PIHCA)) is used in this project.

The nanocarriers can be tailored in a variety of ways, carrying a plethora of different molecules, including imaging agents. One example is loading the NPs with iron particles to enable magnetic resonance imaging (MRI) while therapy is taking place [6]. This combination of therapy and diagnostics is called theranostics, and is a highly desired goal in medicine, allowing for more personalized and effective medical treatment.

One of the possibilities NPs bring to the table as drug carriers, is the ability to exploit the aforementioned EPR effect. By tailoring the size of the NPs, one can increase the amount of drugs that escape from the blood at the tumor sites.

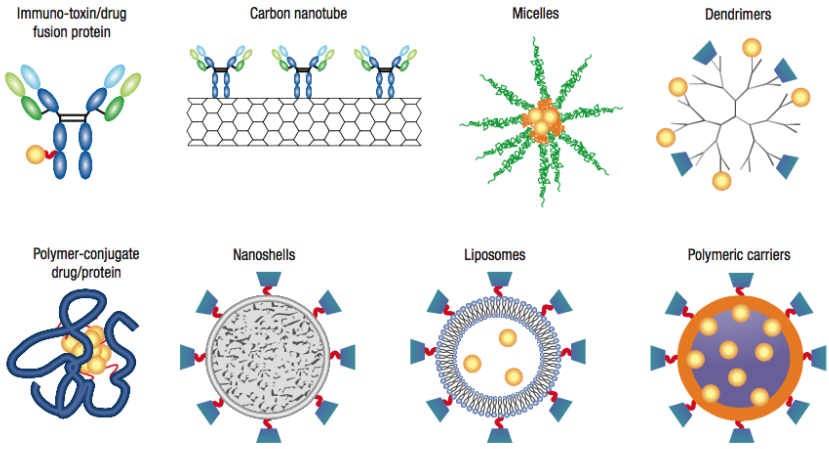

Figure 2: Examples of different types of nanocarriers for targeting cancer. Adapted from [12].

Additionally, because of the other side of the EPR effect, the poor clearance system, the NPs could stay in the tumor for a prolonged time compared to in healthy tissue [9]. Exploiting the EPR effect is a passiv targeting mechanism, as opposed to for example functionalizing the NPs' surface with certain targeting molecules designed to bind to cancer cells, which would be an active targeting mechanism. The NPs can also be functionalized with a molecule designed to hide them from the body, so that they are allowed to circulate in the blood without the risk of our immune system attacking and neutralizing them. One such tactic is adding polyethylene glycol (PEG) to the surface, shielding the NPs from the defence mechanisms of the body by steric stabilization [5]. This is a common approach when increasing circulation time of drug carriers in the body. Clearly, NPs hold much promise as drug carriers, but the approach is, as we shall see, not without its limitations.

2.4 Barriers to drug delivery

An injected drug or drug carrier must travel through the blood, find the tumor, cross the blood vessel wall, travel through the extracellular matrix (ECM) of the tumor and reach the desired cells before it can exact its effect. The road from injection of a drug, to successful delivery into the cell is long and full of obstacles, and a clever and thought-through design is necessary to circumvent these obstacles.

When foreign objects enter the bloodstream, the immune system reacts to them and will try to kill and remove them. NPs can elicit such an immune response, and thus it is necessary to protect the NPs from the immune system

in order to give them time to reach and accumulate at the tumor site [14]. The aim is thus to increase the circulation half-life, which can be achieved by PEGylation of the NPs as described in section 2.3.

When the NPs reach the tumor site, the idea is that they will exploit the EPR effect to enter the tumor. However, the EPR-effect is counteracted by an elevated interstitial fluid pressure resulting from the poor lymphatic drainage that characterizes the tumor tissue. Furthermore, a high collagen density makes diffusion through the tissue difficult, and poor and/or uneven vascularization also poses a problem [15, 10].

In healthy tissue, an evenly distributed vessel network allows each cell to be no more than a few microns away from the nearest blood vessel. In a tumor however, this distance can be more than 100μm [10]. This results in a significant part of the tumor being unaffected by the treatment. Poor penetration into the tumor can be a major problem in cancer treatment. If only the cells closest to the blood vessels are affected by the treatment some cancer cells might survive, and there is a risk that the cancer will never be completely gone. The tumor cells that are not effectively killed could end up developing a resistance towards one or several of the drugs used, which would pose a threat to the patient [12]. A *high* vascular density on the other hand would promote uptake of NPs [10]. Different tumor types differ in all of these parameters, and will thus show different uptake of NPs. Some types even have a variable degree of permeability of vessels, and thus, the distribution of drugs will be heterogeneous throughout the tumor.

2.5 Cellular uptake of nanoparticles

Once the NPs reach the cell, they have to cross the cell membrane. The cell membrane consists of a lipid bilayer containing a plethora of proteins that are essential to membrane and cellular function. The membrane proteins can function as transporters of small molecules, or they can contribute to the membrane's structural properties. Uptake through the membrane can happen through several uptake mechanisms, based on the properties of the entering molecule or particle, such as size, shape, surface charge and surface chemistry. These mechanisms include simple or facilitated diffusion, active transport by transport proteins, or endocytosis. As NPs are so large that they can only enter through endocytosis, it is the only mechanism that will be elaborated on here [2].

Endocytosis is a term describing several slightly different uptake mechanisms, but they all progress as follows: As soon as something initiates the endocytosis, a small segment of the plasma membrane folds inward, and then pinches off to form an endocytic vesicle containing the ingested substances or particles. The endocytic vesicle isolates its contents from the cytosol of the cell. Most of these endocytic vesicles develop into early endosomes and subsequently form lysosomes. The three main types of endocytosis is phagocytosis, receptor-mediated endcytosis, and receptor-independent endocytosis. The opposite mechanism of endocytosis is exocytosis, which expels material from the cell to the outside environment [2].

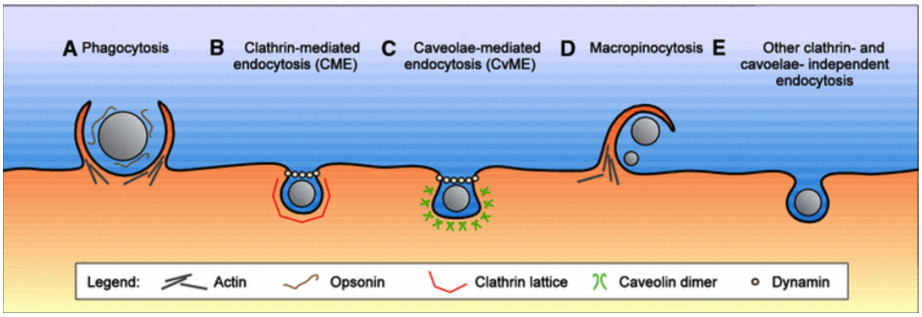

Figure 3: The main internalization pathways for nanocarriers, as described in section section 2.5. Adapted from [16].

Phagocytosis is the ingestion of large particles (larger than half a micron in diameter). This could even include whole microorganisms or other cells. Phagocytosis is for example a critical mechanism for cells of our immune system, such as the macrophages. Receptor-mediated endocytosis, also known as clathrin-dependent endocytosis is another form of endocytosis that uses receptors found on the outside of the plasma membrane to initiate endocytosis. When a specific molecule, or ligand, binds to these receptors, the receptor-ligand complex diffuse laterally in the membrane until it reaches a so-called coated pit. Here, additional proteins are recruited on the inside of the membrane, namely adaptor protein, clathrin, and dynamin. These proteins promotes membrane curvature and invagination of the pit, which results in a pinching off of the invaginated membrane, and the formation of a vesicle. The last endocytosis mechanism is receptor-independent endocytosis. One example of this is fluid-phase endocytosis, which is a kind of pinocytosis, or "cell drinking" for nonspecific internalization of extracellular fluid. This is believed to be a mechanism to control cell volume and surface area, following exocytosis [2].

Once the NPs have successfully made it into the cell, they are degraded, and their contents released. The way NPs are taken up in cells differ depending on the NPs themselves, as well as cell type and external factors such as temperature and pH. Two known properties of NPs that determine uptake are size and surface charge [17]. Lower uptake with increasing NP size has been seen by dos Santos et al. for certain uptake mechanisms [18]. Sulheim et al. showed that PC3 (human prostate tumor) cells and RBE4 (rat brain endothelial) cells displayed different internalization behaviours. Whereas poly(octyl cyanoacrylate) (POCA) NPs were internalized more efficiently than poly(butyl cyanoacrylat) (PBCA) in PC3 cells, the opposite was seen when looking at RBE4 cells [13]. Both PBCA and POCA are part of the PACA family mentioned in section 2.3. It is hard to predict how a certain type of NP will be taken up by a certain cell line. It is also possible that the cell line one is working with is, for some reason, not inclined to internalize the NPs. Even if the cells do internalize the NPs with the anti-cancer drugs, the rate at which this happens might be too low to be helpful

in any real-life situation involving cancer patients. A way to enhance this uptake is therefore desirable, and that is where sonoporation comes in. Sonoporation describes the use of ultrasound to enhance cellular uptake. Before we delve into the specifics of sonoporation, however, a word on ultrasound is appropriate.

2.6 Ultrasound

Sound is molecular vibrations transporting energy from a source, like a loudspeaker, to a receiver, like our ear. A sound wave have certain properties, one of which is the pitch, or the frequency of the vibration. While human beings can hear sounds from approximately 20Hz to 20kHz, the sound spectrum does not begin and end there. Just as there are infrared and ultraviolet light waves that the human eye cannot percieve, there are sound waves below and above these limits. Ultrasound starts at a frequency of about 20kHz, meaning that it is too high-pitched for humans to hear. Ultrasound can be used in medicine for both diagnostics and therapy. The frequency typically ranges from around 1 MHz to 5 MHz, depending on the application [19]. Therapeutic applications use frequencies around 1Mhz, while diagnostic tools use higher frequencies [20]. The medical applications of ultrasound can also be categorized in high- and low-intensity ultrasound. Low-intensity ultrasound is used among other things for imaging and blood flow studies, while high-intensity ultrasound can be used for kidney stone shattering or to destroy a tumor by ablation [21].

The generation of an ultrasound wave usually involves a piezoelectric crystal transducer that gets an input in the form of a voltage waveform, and translates this into linear motion of the transducer's face. This motion then produces pressure waves that are transported through the medium that is in contact with the transducer [19]. The ultrasound travels by transporting information through molecular vibrations, and is thus sensitive to changes in the medium it travels through. Moreover, ultrasound does not travel well through air, and a medium such as water or a gel is required to create a contact between the transducer and the tissue to be exposed [19].

When passing through an interface between different media, the ultrasound wave undergo reflection and refraction. This means that two new waves are created. One that continues into the new media, albeit with a lower intensity and different propagation angle, and one that is reflected back into the current medium. The fraction of the wave that is reflected depends on the acoustic impedance, Z, of the two media, which is given by the following relation:

$$Z = \rho \times c, \tag{1}$$

where ρ is the density of the material, and c is the wave velocity. The fraction of the wave reflected, R, is given by:

$$R = [\frac{Z_1 - Z_2}{Z_1 + Z_2}]^2, \tag{2}$$

where Z_1 is the impedance of the first medium and Z_2 is the impedance of the second medium.

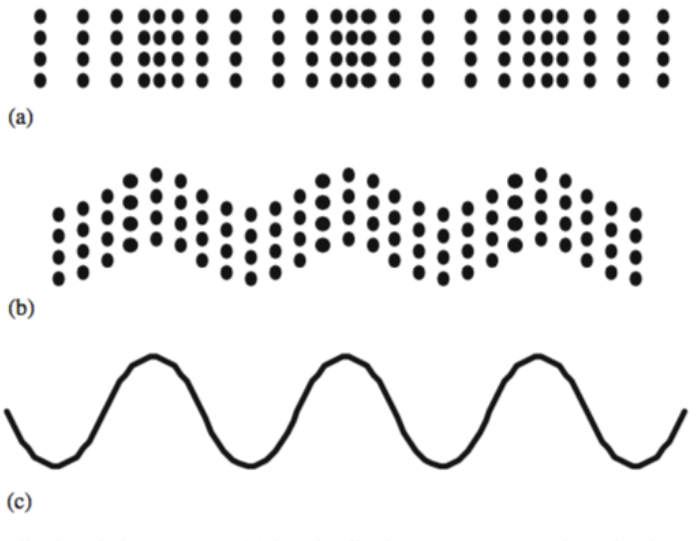

Figure 4: Longitudinal (a) and shear (b) waves. (c) shows a sine wave representation. Adapted from [20].

An acoustic wave can be classified as either a longitudinal wave, or a shear wave. The difference between these two types is in the direction the particles in the medium move relative to the direction of the energy propagation. In a longitudinal wave, the particles are moving back and forth, horizontally, relative to the direction of a wave that also moves horizontally. In a shear wave, however, the particles are moving up and down relative to a horizontally moving wave (figure 4). While a longitudinal wave can occur in any medium, gas, liquid or solid, a shear wave can only occur in solids. In the case of bodily tissue, most of the time only longitudinal waves are applicable because soft tissues are approximated as liquids. Shear waves can, however, propagate in bones [20].

When traveling through a medium, an ultrasonic wave undergoes some energy loss. This is due to frictional forces that disrupt the periodic motion of the molecules oscillating up and down (or back and forth), and thus, part of the energy will dissipate as heat. This is called absorption because the wave energy is absorbed by the medium the wave is propagating through. The absorbance rises with increasing frequency. This is important to keep in mind when using ultrasound in diagnostics, as heat generation in tissue during ultrasonic imaging is usually undesirable. Part of the wave is also dispersed in the medium because of matter inconsistency. This dispersion, together with absorption, causes the wave to lose some of its acoustic energy, an effect called attenuation [21].

Ultrasound travels in waves and thus have certain wave parameters. The amplitude (A) of the wave is the difference between the maximum values of compression and rarefaction (separation of molecules) [20]. A can be expressed in units of length or pressure, describing either maximal distance between

molecules in relation to the rest state, or maximal local pressure, respectively [21]. The wavelength, denoted by λ, describes the distance between two sequential amplitudes, also called a cycle. The period, T, is the time it takes for the wave to travel the equivalent of one wavelength, and is the inverse of the frequency ($T = 1/f$). The wavelength is thus distance per cycle, while the period is time per cycle. The speed of propagation of the wave is what relates λ and T, through the following equation [20]:

$$c = \lambda f, \tag{3}$$

or:

$$c = \frac{\lambda}{T} \tag{4}$$

This wave velocity is dependent on the properties of the medium it is travelling through. The medium's elasticity (K) and its density (ρ) determines the propagation speed as follows [21]:

$$c = (\frac{K}{\rho})^{0.5} \tag{5}$$

The way the wave is shaped when it is generated and transmitted from the transducer is called the generation mode. One such mode is continuous wave mode. In this mode, the transducer is continually excited by a constant electrical signal. The wave generated is continuous and has the same frequency as the electrical wave of the input signal to the transducer. Another generation mode is a pulsed mode, in which the wave is switched on for a certain duration, and then switched off for a much longer duration. This is done by exciting the ultrasound transducer with very short electrical signals, and waiting a certain amount of time before repeating. This is called a pulsed wave mode and is illustrated in figure 5. The length of the "on" mode can be given in terms of number of cycles. If this number of cycles is N, then the total duration of one pulse (τ) is [20]:

$$\tau = NT = \frac{N}{f} \tag{6}$$

The time it takes from the start of one pulse to the start of the next pulse is called the pulse repetition period (PRP). The number of pulse repetitions per time unit is called the pulse repetition frequency (PRF). PRP and PRF thus has the same relationship as T and f. The ratio of pulse duration to the PRP is called the duty factor (DF), or duty cycle (DC). In other words, the DC is the fractional amount of time that the signal is "on", and is given by:

$$DC = \frac{\tau}{PRP} = \tau PRF \tag{7}$$

The final concept that has to be understood when working with ultrasound is the mechanical index (MI). The concept of MI was proposed in the early

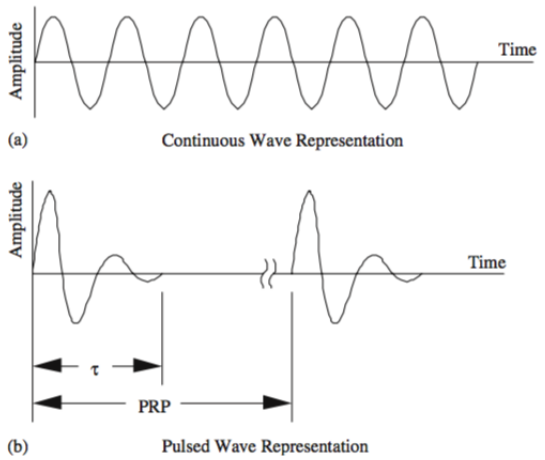

Figure 5: Schematic representation of continuous wave (a) and pulsed wave (b) ultrasound. Adapted from [20].

1990s [22] and estimates the probability of an adverse, non-thermal (mechanical) biological effect in tissue exposed to ultrasound. The MI also indicates the likelihood of inertial cavitation (section 2.7.3). The higher the MI, the higher the probability of inertial cavitation. The MI can be expressed as

$$MI = \frac{PNP}{\sqrt{f}} \tag{8}$$

where PNP is the peak negative pressure in MPa, and f is the frequency in MHz. The peak negative pressure is the same as the peak rarefactional pressure, p_r, and describes the pressure on particles carrying the acoustic wave when they are displaced maximally from the resting position [23].

2.6.1 Microbubbles

The effect of ultrasound on microbubbles (MBs) is an essential part of this project. Before the effects of ultrasound on MBs and tissue is described, however, a word on MBs is appropriate. MBs are the most commonly used ultrasound contrast agent for molecular imaging. Since the 1990s, however, their application has extended beyond diagnostics and into the area of therapeutics, as a tool to enchance drug delivery. MBs oscillate under the influence of ultrasound, a response which causes shear stresses and jet streams in surrounding tissue. This leads to increased extravasation into and throughout the tumor tissue [6] and can even be used to get drugs through the notoriously tight blood-brain barrier [24].

MBs are usually in the size range of 1-8 μm [25], and can be free or encapsulated MBs (EMB) [23]. Free bubbles are usually cavities filled with air

or other gases, or gas vapor from surrounding liquid. The free MBs have no artificial boundaries to prevent leakage of gas from the bubbles, and are less stable than EMBs. EMBs consist of a gas core stabilized by a shell of phospholipids, biocompatible polymers, proteins, etc. The gas core is usually air, nitrogen, or inert heavy gases such as perfluoropropane, -butane, -hexane, or sulfur hexafluoride [25]. These heavy gases usually show better stability than air or nitrogen, which leads to a longer half-life in the blood, thus making them better suited as MB cores [25]. The MBs' response to ultrasound depends on their nucleus size [22], as well as the MB shell.

The flexibility of the MB in particular will have a big impact on the effect of ultrasound treatment. Lipid-shelled MBs are quite flexible when compared to stiffer shells made from proteins or polymers. This flexibility allows the lipid-shell MBs to oscillate at lower acoustic pressures. When they rupture, they fragment into smaller bubbles which stay centered around the intitial bubble. Hard-shelled MBs mainly respond to ultrasound with higher acoustic pressures. Their rupture through a process called sonic cracking. This occurs through a small defect in the shell, with a subsequent violent gas stream being propelled a few microns into the surrounding medium. This creates strong effects and large pores, but only above a certain threshold. More flexible MBs can oscillate under a wider range of ultrasonic pressures, leading to different effects than hard-shelled MBs can elicit, including stable cavitation which can lead to sonoporation or enhanced endocytosis. In addition to this, the MB size also affects the results, with the respons being higher around the MBs' resonant radius. [26, 27, 28, 29]

Many types of MBs exist, both commerically available types and "home made" MBs. Two types of MBs were used in this project. The main focus was on MBs stabilized by a shell of NPs, synthesized and provided by SINTEF [6]. For comparison, comercially available Sonazoid MBs were used. These bubbles are a type of lipid bubbles consisting of a shell of hydrogenated egg phosphatidyl serine (HEPS). More details on these MBs and NPs, and their synthesis can be found in section 3.5.

2.7 Effects of ultrasound on tissue and microbubbles

Ultrasound for imaging and ultrasound for therapy are, as mentioned, used very differently. Images of tissue is obtained by transmitting a pulse into a tissue, which is then partially reflected at the interface between different tissue structures. The reflected waves are reconstructed to form an image on a computer screen. For a certain intensity, the higher the frequency, the higher the resolution of the image [21]. In addition, heating effects of ultrasound are undesirable in diagnostics, as it could potentially cause harm to the patient. This limits the wave intensity that can be used. For therpeutics, however, the situation is quite different. The frequency and intensity is in the other end of the spectra with respect to diagnostic ultrasound, and thermal effects might in fact be the primary goal of the treatment. The effects of ultrasound on biological tissue can roughly be categorized as thermal or non-thermal effects. Non-thermal effects

include acoustic radiation force, as well as cavitation.

2.7.1 Thermal effects

Thermal effects arise due to the phenomenon of attenuation discussed earlier. Attenuation happens partly due to absorption and partly due to scattering (only about 10% is due to scattering). Whereas scattering can be thought of as the part of the wave that changes direction, absorption can be thought of as the part of the wave that is converted into heat. This happens, as mentioned in section 2.6, due to frictional forces in the tissue that the wave is penetrating. Part of the wave energy is thus lost from the wave and results in an elevated tissue temperature. For diagnostic ultrasound this is an undesirable effect, as it can cause damage to the tissue. For therapeutic ultrasound however, this heating has been used for a plethora of purposes [20].

The heating of the tissue, also known as hyperthermia, has been used for many years for a wide range of applications. These range from treating musculoskeletal pains, soft tissue injury and osteoarthritis [30], and it has also been used for drug delivery. The heat can be used to melt drug containing liposomes, thus releasing its contents, or using even higher temperatures to directly kill the cancer cells by ablation [31]. The effects of this controlled hyperthermia includes increased drug release, diffusion, permeation or even cell uptake, and the heating becomes a mechanism for controlled and local treatment [19].

2.7.2 Non-thermal effects

Radiation force
As the acoustic wave propagates through tissue, not all of the lost energy is converted to heat. Some of the wave's momentum is transferred to the tissue through which it is propagating. This transfer of momentum creates a unidirectional force, also known as acoustic radiation force. This force is proportional to the absorption coefficient of the medium and the rate of energy being applied, and inversely proportional to the rate of propagation of the ultrasonic wave in the medium [15]. The displacement that the radiation force causes may cause shear stress between diplaced and non-displaced tissue, which in turn will lead to a strain. This strain may lead to gaps between endothelial cells and widening of intracellular spaces in epithelial tissue [32]. This, in turn, can increase the amount of drugs escaping from blood vessels, which is highly beneficial for drug delivery systems. In a fluid medium, the radiation forces can result in a steady flow, known as acoustic streaming. This streaming has been shown to reduce heating in tissue when exposed to ultrasound because of an increased convective heat loss. Also, acoustic streaming can increase the mass transport of NPs in the medium [15]. The effect of this mass transport depends of the particles being affected by the ultrasound, with larger particles experiencing the greatest effect. MBs are also affected in this way. Another non-thermal effect of ultrasound, which is particularly pertinent when working with NPs and MBs, is aggregation. During ultrasound treatment, because of interactions between

the MBs, aggregation can occur due to secondary Bjerknes forces. For a more comprehensive look at this phenomenon, the reader is referred to [33].

2.7.3 Acoustic cavitation

The last effect of ultrasound on biological tissue that will be covered here is acoustic cavitation. Acoustic cavitation refers to the response of small, micrometer-sized, gas filled bubbles (microbubbles (MB)) under the influence of ultrasound. When looking purely at the potential to enhance drug delivery, acoustic cavitation of MBs is considered the most important effect of ultrasound [15]. Acoustic cavitation of MBs can generally be divided into two categories: Stable cavitation and inertial cavitation. These two mechanisms lead to quite different physiological effects, both of which can contribute to cellular uptake of NPs.

Stable cavitation
During cavitation of MBs, there is gas influx during expansion of the bubbles, and gas efflux during compression (figure 6). The net gas influx during one expansion/compression cycle is zero. However, the expansion phase can extend, leading to a net gas influx, which will continue until the bubble reaches its resonant size. Once reached, the bubble will demonstrate stable, low amplitude oscillation. This oscillation creates a flow around the MB, which is called microstreaming. If the bubble is sufficiently close to a cell, this microstreaming will cause the cell to experience a shear stress. The stress level depends on the ultrasound parameters, but is quite high compared to the stress the cell experiences because of blood flow [26]. This stress can lead to two main mechanisms in the cell: The formation of small pores, and endocytosis. The resulting mechanism depends on the size of the particles entering the cell, endocytosis being the dominant mechanism for larger molecules, and pore formation dominanting for smaller molecules [34]. The cavitation and its resulting microstreaming works by pushing and pulling on the nearby cell membrane and disrupting the membrane integrity, leading to one of these two effects.

Inertial cavitation
Using higher ultrasound intensities can cause the MBs to grow during the low pressure phase until they collapse. This type of cavitation is called inertial cavitation, and can lead to the fragmentation of the bubbles into smaller bubbles. During the collapse, shock waves can be generated in the fluid, and a jet of gas can be propelled out of the collapsing bubble [26]. This jet stream that is created can work as a syringe, puncturing the cell membrane, leading to a pore such as the ones that occur during stable cavitation, although usually bigger.

For stable cavitation to have an effect on nearby cells, direct contact is required between cell and MB [35, 36]. With inertial cavitation, however, this effect reaches over a longer distance. The added range, although useful, is however quite small, and the distance between cell and MB should not exceed the MB diameter [26]. Close proximity between cells and bubbles is therefore

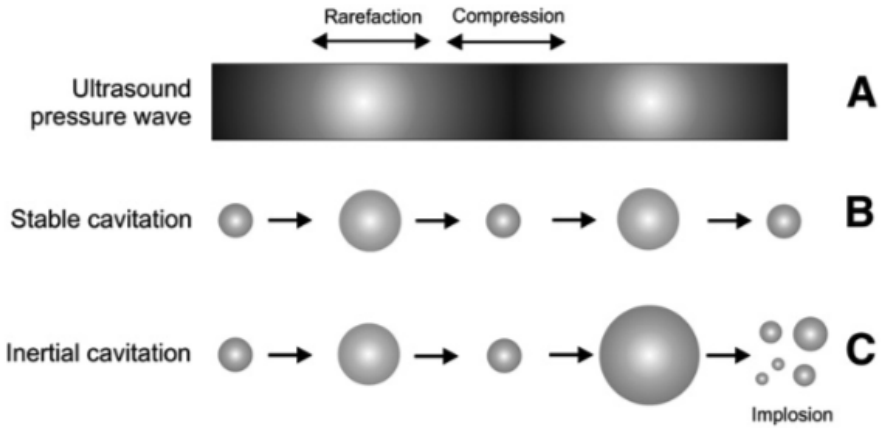

Figure 6: Stable (B) and inertial (C) cavitation in response to an ultrasound wave (A). Adapted from [26].

crucial.

The size of the pores resulting from inertial cavitation is generally larger than what is seen with stable cavitation, with sizes into the micrometer range having been observed after inertial cavitation. For stable cavitation, pore sizes of up to around 50nm have been observed. For both inertial and stable cavitation, the pores reseal within seconds [26]. This underlines the importance of close proximity between cells, MBs and the molecules or particles to be taken up.

2.8 Sonoporation

When talking about ultrasound in medicine, most people probably think of a woman getting a check-up on her unborn child. The use of ultrasound in diagnostics is well known. However, a new application of ultrasound has emerged. Since the 1990's, ultrasound has been shown to facilitate transport of membrane impermeable compounds into living cells. The addition of MBs further enhances this effect, because of the way the MBs respond when exposed to the sound waves, as described in the preceding sections. The combination of MBs and ultrasound can be used in several stages of the drug delivery process. This includes assisting drug escape from blood vessels and extravasation through the tumor ECM, and enhancing cellular uptake of the drugs [26]. Using ultrasound on MBs can lead to small, transient pores in cell membranes, through which drugs can enter the cell. This process is called sonoporation. The combination of MBs and ultrasound can also lead to enhanced endocytosis by affected cells, which can also aid in cellular uptake of drugs. The exact mechanism leading to the enhanced cellular uptake after ultrasound treatment can be difficult to pinpoint. In most cases there is probably a combination of mechanisms responsible.

The aim of sonoporation is to enhance cellular uptake of NPs or molecules that otherwise would not be taken up, or would only be taken up in small doses. Not only NPs and molecules are taken up, as there are reports of entire intact MBs entering the cells, probably as a result of acoustic radiation forces. Recently, De Cock et al. [37] reported a new phenomenon they termed sonoprinting, in which MBs deposit its NP shell onto surrounding cells. The cells then take up the NPs, and although the exact uptake mechanism is unclear, they hypothesize that it might be due to lipid fusion of the MB shell fragments and the cell membrane. Much research on sonoporation exists. Effects of varying MIs, pulse lengths, PRF and other parameters have been investigated. So has the biophysical effects on the cell resulting from the ultrasound treatment. Pore sized, resealing times and cellular uptake have all been measured. Much has been done, but there are two important aspects separating most, if not all of that research, with this thesis. First, most papers on sonoporation so far have aimed at enhancing uptake of small molecules, such as dextrans, calcein, etc. Comparatively few have used NPs, which due to their size are much harder to get into cells through pores. Second, most papers use commercially available MBs, which are usually made of a lipid shell. Additionally, some MBs are made up of polymers or proteins. However, to the best of the authors knowledge, no research has been done using MBs stabilized by a shell of NPs, such as the MBs used in this thesis. [26]

One important takeaway from this is that sonoporation, although being a very exciting and promising technique, is difficult to understand. Due to the amount of variables, both in ultrasonic parameters and MB/NP composition, there will inevitably be quite a bit of trying and failing before a suitable set-up for one's specific experiment is found. It is also important to understand that as exciting as sonoporation is, at this time it is not clinically relevant. For sonoporation to be possible there needs to be MBs present, but MBs are too big to escape from the blood vessels, even from leaky ones. Some possible solutions to this issue are in progress, such as using nanoemulsions which, after extravasation into the tumor, can expand into a gaseous phase. Another approach could be to use a MBs that, when collapsing, breaks up into smaller MBs rather than being completely dissolved. Additionally, there are some approaches to using sonoporation outside of the body, for example for treatment of dendritic cells for immunotherapy [38].

2.9 Confocal laser scanning microscopy

Cells and tissue is often imaged with the help of fluorescent signals, often to track the path of a labeled particle or molecule. When imaging cells, which are often relatively thick and rounded, with conventional widefield optical systems, the result might not be good. Bright, fluorescent signal from objects lying outside the focal plane of interest will increase the background signal of the image and lead to low contrast and poor quality of the images [39].

The brilliance of the confocal laser scanning microscope (CLSM) is its ability to eliminate out-of-focus signal from the final image using a focused, scanning

laser beam, and a small pinhole aperture in front of the detector. This allows the cross-sectional imaging of live cells and other samples, as well as the possibility to aquire a 3D-image of the sample.

The resolution of the CLSM is not comparable that of an electron microscope, but better than what is achieved with conventional widefield microscopes, thereby bridging these two technologies [40].

In a CLSM system, epi-illumination is used. This means that the light source and the detector are on the same side of the sample, separated from it by the objective which works both as an objective and a condenser. The light source is a focused laser beam, which raster scans the sample from side to side to form an image. The laser excites the fluorescent dyes in the sample, which then emits a fluorescent signal. This signal goes through the aperture pinhole only if it originates from the focal plane, and is blocked if not. On the other side of the pinhole is a photomultiplier tube (PMT) that functions as a detector. Because of the design of the system, the PMT does not receive an image, but rather a fluorescent signal. The PMT then translates the intensity of this signal into a voltage. A computer then builds up an images based on the voltages received from the PMT and displays it on a monitor [39].

There are several noteworthy advantages of a CLSM system over a traditional widefield system. One of these advantages is the possibility to create a 3D-image. Because the microscope strictly detects signal from a single z-plane, several such images can be digitally stacked on top of each other to create a z-stack, or a z-series. The result is a 3D-view of your sample, which is a powerful tool when studying cells. This 3D-model is constructed by advanced computer software - which is the second big advantage of the CLSM. The software can process the images in several ways to increase their usefulness. One example is transverse x-z or y-z cross-sectional views of the 3D-model, which makes it seem as if the sample has been cut in a plane parallel to the optical axis. This is a useful tool when studying uptake of NPs or MBs, to uncover whether they are inside the cell, or just bound to the extracellular side of the membrane [39, 40].

Other advantages of the CLSM include the use of filters. Different filters can be used for the different lasers being applied, thereby selecting only the emission area of interest. In addition, parameters such as gain, laser intensity, scan speed, number of captures before averaging, etc. can be tailored to suit one's specific need, further improving the resulting images. A schematic of the workings of a CLSM can be seen in figure 7.

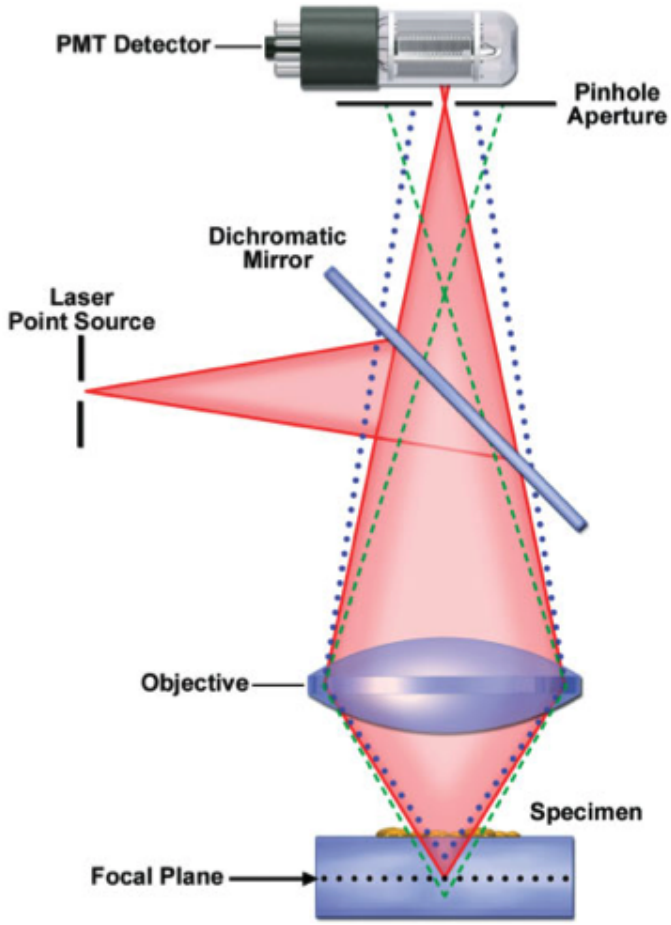

Figure 7: Schematic of the optical pathway and working principle of a confocal laser scanning microscope. Adapted from [39].

3 Materials and Methods

This master thesis is a continuation of a project thesis on sonoporation carried out during the fall of 2016. The final experiment in that project, in which cellular uptake of NPs was seen, was therefore the starting point of this thesis. Many of the parameters used in the beginning of this thesis are the same as what was used in the end of the project thesis.

3.1 Cell cultivation

Human prostatic adenocarcinoma (PC3) cells (American Type Culture Collection) were cultured in Dulbecco's Modified Eagle Medium (DMEM, Gibco by Life Technologies) supplemented with 10% fetal bovine serum (FBS, Sigma Aldrich) and 1% Penicillin Streptomycin. The cells were grown in a 75 cm^2 flask (Tissue Culture Flask, VWR) with 15 mL growth medium and incubated at 37°C with 5% CO_2. Cells were passaged onto a new flask every monday and friday, and the medium was changed every wednesday. Passaging was done by removing the old medium, and washing the cells with 5 mL PBS (Sigma Aldrich). PBS was removed and 3 mL of 0.25%/0.02% trypsin/EDTA (Sigma Aldrich) was added, and the flask incubated at 37°C for 2-3 minutes until the cells had detached from the flask surface, which was confirmed by light microscopy (Leica DMIL). Trypsination was stopped by addition of 10 mL of growth medium. 10 mL of suspension was then transferred to a 15 mL centrifuge tube (Corning Centristar), and sentrifuged for 5 minutes at 1500 rpm (Heraeus Instruments, Megafuge 1.0). Prior to sentrifugation, a droplet of suspension was transferred to a Bürker chamber and the cells were counted using a light microscope (Leica DMIL). After sentrifugation the supernatant was removed from the tube, and new medium was added so that the concentration was $1{\cdot}10^6$ cells/mL suspension. $1.5{\cdot}10^6$ cells were transferred to a new flask containing 13.5 mL, giving a total of 15 mL, and incubated again at 37°C.

3.2 Seeding of cells in CLINIcell

CLINIcell cell culture chamber (Mabio) was used for cell growth and treatment. The CLINIcell has two optically and acoustically transparent polycarbonate gas permeable membranes enclosing a volume of 11 mL. The growth surface is 25 cm^2 per membrane, and the two inner membrane surfaces are plasma treated to promote cell adhesion [41]. Approximately 400'000 to 500'000 cells were seeded in a CLINIcell four days prior to the experiment, following routine cell passaging, to obtain a confluent layer on the day of the experiment. The CLINIcell was filled by injecting the different solutions through the CLINIcell's inlets (figure 8). The solutions were slowly and carefully injected into the chamber to ensure even distribution of cells in the case of seeding, and to protect the cells in the case of medium change and during experiments. The CLINIcell was emptied by opening both inlets and pouring the solution out of the CLINIcell. To avoid air bubbles during injection, 12 mL of solution was injected into the container.

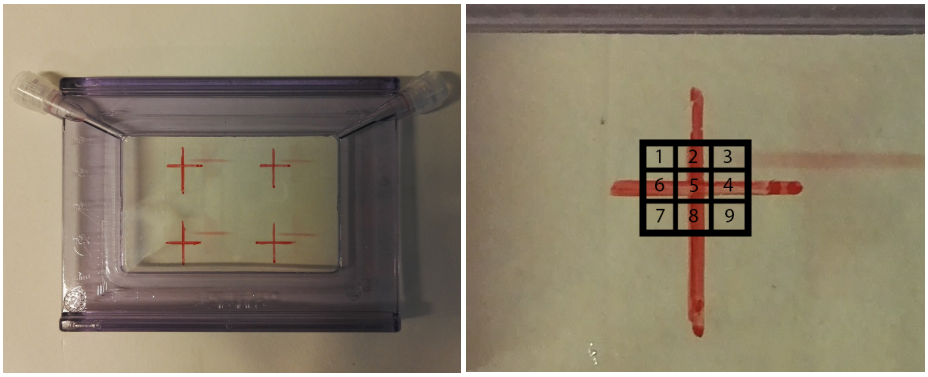

(a) **(b)**

Figure 8: (a) shows the CLINIcell cell culture chamber, in which cells were seeded. Two optically and acoustically transparent membranes allow for inspection of the cells while they are growing, as well as ultrasound treatment. The two in/outlets of the CLINIcell can be seen at the top corners. The four red crosses indicate the fixed four treatment areas. (b) shows a close-up of a CLINIcell with the 3x3 imaging grid marked on one of the treatment areas. The numbers illustrate the order in which the imaging was performed.

The excess solution made it possible to gently squeeze the two membranes of the CLINIcell slightly together, pushing out the air and some excess solution. After injection of cell suspension into the CLINIcell, the CLINIcell was placed in the same incubator as the tissue culture flasks in section 3.1. Note: The CLINIcell system has a cap with a valve on one of its inlets that would make removal of air easier, but this valve could not be used because of its size, as it would cause the CLINIcell to not fit in its sample holder during treatment or on the microscope stage during imaging.

3.3 Experimental setup

The experiments were performed in a tank to allow complete submersion of the ultrasound transducer and the CLINIcell in water. An image of the setup can be seen in figure 9. The CLINIcell, containing a confluent or near confluent layer of cells, was placed in the sample holder above the transducer. The distance between the transducer and the sample was set to 125 mm to make sure the cells were in the focal position of the ultrasound beam. The sample holder allowed for a lateral movement of the CLINIcell of about 2-3 cm, allowing two different exposure areas in the x-direction. As the holder was, by design, off-center in the tank, two additional exposure areas could be obtained by rotating the CLINIcell 180° in the holder. This resulted in four different treatment areas, as shown in figure 8. Crosses were drawn with permanent marker on the membrane not covered by cells, to easily see where the ultrasound treated areas were, while still allowing for clear and undisturbed imaging of the cells. After placing the

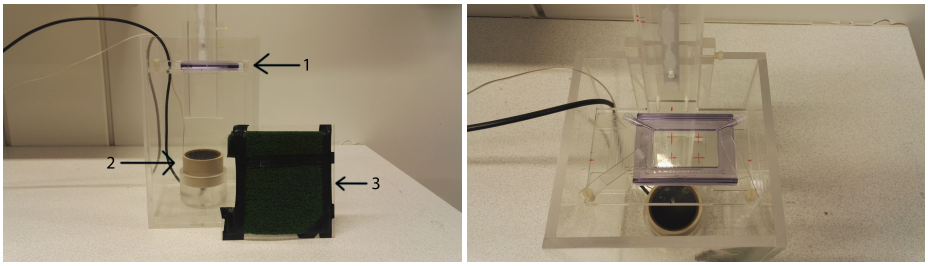

(a) **(b)**

Figure 9: Front (a) and top (b) view of the experimental setup, with the plexiglass tank that was filled with water. 1) Sample holder with the CLINIcell (purple) mounted in place; 2) Ultrasound transducer; 3) Absorbing lid.

ultrasound transducer in its holder in the tank, the tank was filled with degassed water until the water level reached a few centimeters above the sample holder. Water was degassed by filling a small tank with as hot water as possible from the tap, and leaving it for at least 24 h before use. The prepared CLINIcell was carefully placed in the holder, submerged at a steep angle to avoid gathering of gasbubbles underneath it, as this could disturb the ultrasound wave. After successful placement of the CLINIcell, the tank was completely filled with water, and an absorber lid was placed on top, without any gap between the lid and the water surface. A visual inspection was performed before exposure to make sure there were no bubbles in the ultrasound path.

A signal generator (Trueform 33500B Series Waveform Generator, Agilent), an amplifier (Model 2100L-1911 RF Power Amplifier, ENI) and a transducer (Imasonic) was connected in series to produce the ultrasound signal. The signal generated was set to a frequency of 1 MHz, which is the center frequency of the transducer. The amplitude of the output signal from the signal generator was varied between 20 and 282 millivolts peak-to-peak (mVpp), which corresponds to an output from the transducer - in mechanical index units - of 0.1 to 1.12 MI. Pulsed ultrasound was used, with a PRF of 50Hz (PRP of 20ms) and 100 cycles. This corresponds to a duty cycle of 0.5%. Some exposures were performed with a PRF of 100Hz and 1000 cycles, corresponding to a duty cycle of 10%. In an attempt to simplify conversion between parameters used in these experiments, and parameters used in the various papers referred to in this thesis, table 1 was made.

3.4 Experiment preparations and ultrasound treatment

On the day of the experiment, the CLINIcell was inspected in a light microscope (Leica DMIL) to ensure that the cell layer was confluent or near confluent. The suspension was then carefully removed from the CLINIcell, and replaced with 10 mL of medium containing the MBs and NPs. The CLINIcell was then flipped upside down and placed in the tank for 30 minutes, to allow the MBs to

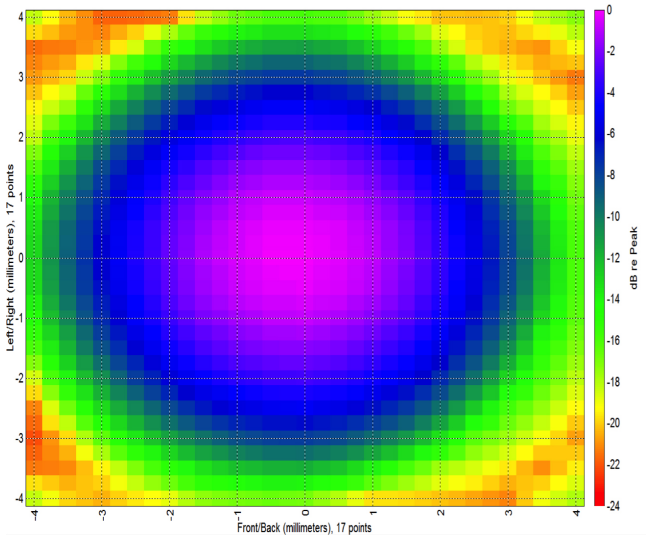

Figure 10: Pressure profile of the 1 MHz Imasonic transducer. The focal diamter (within a 3 dB reduction) is around 3 mm.

rise towards the cells to get the close contact between cells and MBs that the experiment requires. A waiting period of 30 minutes was found to be sufficient, confirmed by light microscopy during the project thesis preceding this work.

Once the confluent CLINIcell was placed in the sample holder in the tank, the sample holder position was adjusted so the distance between the ultrasound transducer and the cells was 125 mm, the focal length of the transducer, after which treatment could commence. Ultrasound exposure was done in four successive treatments, one for each exposure area. Each area was treated for one minute. In every experiment, one treatment area was used for one ultrasound setting, so that four different ultrasound setting could be compared for each CLINIcell.

Once all exposures were done, the CLINIcell was removed from the tank. The MB/NP-containing medium was then removed from the CLINIcell and replaced with medium containing Cell Mask for 5 minutes in order to stain the cells. After 5 minutes, the medium was again removed from the CLINIcell and replaced with PBS (Sigma Aldrich), before imaging could begin.

No fixation of cells was performed due to findings from the project thesis concluding that chemical fixation of the cells after ultrasound treatment somehow impares cellular uptake of NPs.

The ultrasound treatments were, unless otherwise stated, performed at a room keeping a constant temperature of 37°C. This ensured that all components involved in the experiment kept the same temperature, and that the cells were kept at their preferred temperature for as long as possible. All chemicals used in the experiment were heated to 37°C prior to use. One experiment was done

Table 1: This table is meant to aid conversion between different expressions of ultrasonic pressure applied in various papers referred to in this thesis. Only values that have been used in this project are included.

Amplitude signal generator (mVpp)	Output from amplifier (Vpp)	PNP in center (MPa)	MI
20	7.5	0.1	0.1
40	15.2	0.2	0.2
65	24.4	0.3	0.3
70	26.3	0.32	0.32
100	37.2	0.45	0.45
141	52.5	0.59	0.59
200	75	0.85	0.85
282	104.5	1.12	1.12

in a cool storage room keeping a temperature of 4°C. In this case, all chemicals where cooled to 4°C before use.

To determine whether potential uptake of NPs was due to the ultrasound treatment or simply due to normal endocytosis, a control sample was made. This control CLINIcell was treated exactly like every other CLINIcell in this project, except that it did not receive ultrasound treatment. Instead, the sample was left with the solution containing MBs and NPs for the same amount of time as the treatment would take, before removing the medium and replacing it with PBS.

3.5 Microbubbles and nanoparticles

MBs and NPs were provided by SINTEF. Biocompatible and biodegradable PEGylated poly(isohexyl cyanoacrylate) (PIHCA) NPs were synthesized by the miniemulsion polymerization described in [6]. The fluorescent dye Nile Red 668 (NR668, modified NileRed, custom synthesis, 0.5wt%) was added to the NPs for imaging purposes.

NP-MB complexes were made by self-assembly of the NPs (1 wt%, 10 mg/ml) at the gas-water interface by the addition of 0.5% casein in PBS and vigorous stirring using an ultra-turrax (IKAWerke, Germany). For increased circulation time, perfluoropropane was used instead of air. Average MB diameter, size distribution and concentration was determined using light microscopy and subsequent image analysis in ImageJ. Average NP size was 177 nm diameter. Average MB size varied slightly between experiments, but were generally around 2.5 μm in diameter.

A concentration of about 10 MBs per cell in the CLINIcell was used, corresponding to about 15 million MBs for a confluent CLINIcell. This was found, through optical microscopy during the project thesis, to be a suitable amount of MBs ensuring that most cells are in contact with one or a few MBs, without

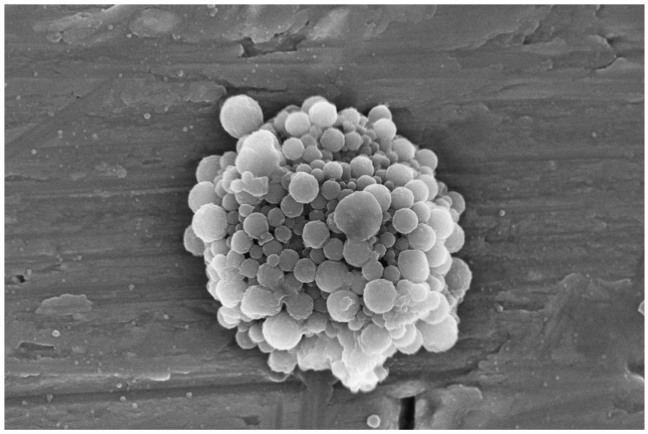

Figure 11: Scanning electron microscopy image of the kind of MB used in this thesis. The small spheres seen are NPs, and together they make up one MB. Image: SINTEF

leading to MB aggregates. The desired amount of MBs was added to a 50 mL centrifuge tube (Corning Centristar) containing 12 mL of DMEM, from which 10 mL was extracted and injected into the CLINIcell during the experiment.

Due to the manufacturing process, there will be a high amount of free NPs in the MB solution. The medium injected into the CLINIcell thus does not only contain MBs. Only about 1% of the NPs in the solution are stabilizing MBs. The other 99% are free NPs.

3.6 Staining

To be able to visualise the cells and the NPs in a fluorescent microscope, two dyes were used. The NPs were prepared by SINTEF and contained Nile Red 668 (NR668), as described in section 3.5. NR668 was excited using a 488 nm laser. To see wheter potential NPs are inside or outside the cells, staining of the cell membrane was done using Cell Mask Deep Red plasma membrane stain (Thermo Scientific). Cell Mask Deep Red was excited using a 640 nm laser. A Cell Mask concentration of 2.5μg/mL was used, as this was reported to be a suitable concentration (personal communication). Cell Mask was prepared in a 50 mL centrifuge tube (Corning Centristar), containing 12 mL of DMEM, from which 10 mL was extracted and injected into the CLINIcell during the experiment.

3.7 Co-incubation of Sonazoid microbubbles and free nanoparticles

For the experiments using co-incubation of free NPs and MBs, commercially available Sonazoid MBs were used (Phoenix solutions). Sonazoid MBs are stabilized by a hydrogenated egg phosphatidyl serine (HEPS) shell, which puts

it it the lipid MB category. A vial of freeze-dried microbubbles, $2.4 \cdot 10^9$ in total, were diluted with 2 mL of PBS, and the solution homogenized by careful flipping of the vial for 60 seconds. Approximately 15 million microbubbles were immediately extracted from the vial and added to 12 mL of medium, similar to the approach described above. NPs were again provided by SINTEF, but this time in a solution of free NPs, with no MBs. The solution was diluted to obtain the same concentration of NPs as in the experiments using NP-stabilized MBs, after which NPs were extracted and added to the medium containing the Sonazoid MBs. This solution was injected into the CLINIcell at the same time and in the same manner as when using the MB solution described above.

3.8 Qualitative inspection of uptake

The result of the ultrasound treatment was evaluated with a confocal laser scanning microscope (LSM800, Zeiss). For qualitative inspection a 40x water immersion objective was preferred as the goal was careful inspection of the cells. Imaging of all cells, both qualitative and quantitative, was performed at room temperature, even in the case where the treatment was performed at 4°C.

Initially, a manual scan of the sample was performed using the occulars of the microscope to look for fluorescent dots. During this step, the sample was illuminated by an external light source (HXP 120 Mercury lamp, Kübler Codix) and a filter cube was used to excite only the NPs. The cells were illuminated by an additional light source, so that cells of interest - i.e. cells that looked like they contained NPs - could be identified. By adjusting the focus the fluorescent dots that were encountered were determined to be either inside, or just above/below the cells. Once a cell of interest was encountered, a z-series was aquired using the microscope's computer software. A 488 nm laser was used to exite the Nile Red 668 of the NPs, and a 640 nm laser to excite the Cell Mask staining the cell membranes. To remove the autofluorescence of the cells from the image, a filter was added, selectively filtering out any signal from the Nile Red below 590 nm, thus removing most of the autofluorescence. After a z-series was aquired, the location of the observed NPs relative to the cell was evaluated through reconstitution of a 3D-image, different cross-sections of the cells, or a maximum intensity projection, all features of the imaging software.

The images at the treated areas of the samples were taken within a few milimeters from the center of treatment. As cells can move during and after treatment, and because there might be an effect of the treatment even outside the focal diameter of the ultrasound beam, the region of interest was somewhat bigger than the focal diameter (3 mm). The field of view was moved slowly from left to right, and stepwise from top to bottom at each turn of the lateral scan. Images were taken of cells of interest, meaning cells showing uptake. Control images were taken at untreated areas of the CLINIcell, at least 2 cm from each treatment area, ensuring no effect of the ultrasound treatment in the imaged control area.

3.9 Quantitative inspection of uptake

Images obtaind for quantitative analysis was taken with the same settings as the ones intended for qualitative inspection, but with a 25x multi-immersion objective, used with a water droplet. This objective was chosen to get overview images of as many cells as possible while still seeing the NPs in and around the cells. 9 z-series images were taken at each treatment area in a 3x3 grid, as shown in figure 8. The first image was taken at the same place relative to the treatment center each time. Similarly, 9 z-series was taken at untreated areas of each CLINIcell, in order to obtain a control reference. The imaging was unbiased, and the images were taken regardless of the visible presence of ingested NPs. The only exception was in cases were an image coincided with an area of the CLINIcell with no or very few cells. In these cases, the imaging area was moved as little as possible to ensure the presence of cells, but still without concideration of the amount of NPs present in the imaging area. Capturing each image took from two to four minutes, depending on the amount of steps in the z-series. Including movement of the imaging area, focusing and setting the z-range for each image, imaging of an entire treatment area lasted anywhere from 45 to 90 minutes. Imaging of an entire CLINIcell, including control area, therefore took between three and six hours. For all experiments with increasing MI, imaging started with the lowest MI and was performed in order of increasing MI, ending with the control area.

The images were analysed in MATLAB using a script written by Astrid Bjørkøy of the Department of Physics at NTNU. The z-series were split into two channels, one for the Cell Mask fluorescence and one for the Nile Red of the NPs. An intensity threshold above and below which the fluorescent signal was counted or not counted, respectively, was set manually. Binary images were then created, like the ones shown in figure 12. Using these two binary stacks the analysis looked at each NP and determined whether it was inside or outside a cell, or colocalized with a cell membrane. The output of the script included both number of NPs and number of NP *pixels*. Only the number of NP pixels is used in this thesis, as it gives the best indication of the amount of NP taken up by cells. Next, the amount of cells present in each image, in terms of number of pixels, was analysed. The amount of NPs was then divided by the amount of cells, in order to get a measure of amount of NPs per amount of cell. This was done to account for the differences in the number of cells in each image. As this ratio is a very small number, the value was multiplied by 10^4. The values presented in the result section is therefor the number of NP pixels per cell pixel multiplied by 10^4.

The data from the analysis was processed in Microsoft Excel. Data from the nine images of each treatment area was averaged, and the standard deviation (SD) was calculated. In the representations of two or more trials combined (as seen in section 4), data from all images of each treatment was averaged, rather than averaging the averages of each trial, and likewise with regards to SD. In the data sets from some treatments there were sometimes found outliers, for example a very high amount of uptake in the control areas. In these cases,

the images were reviewed. In the cases were the uptake was clearly due to artefacts of the imaging or the analysis (like external aggregates being counted as ingested; see section 4), these images were removed from the calculations. The number of images analysed will be indicated in each plot in the results.

Representations of the average of the treatment areas (and controls) were prepared in Excel, and two-sample student t-tests with a significance level of 0.05 were performed to evaluate significance. All results and observations referred to as significant in this thesis thus have a p-value < 0.05. Significance in figures are indicated by a star above the uptake bar.

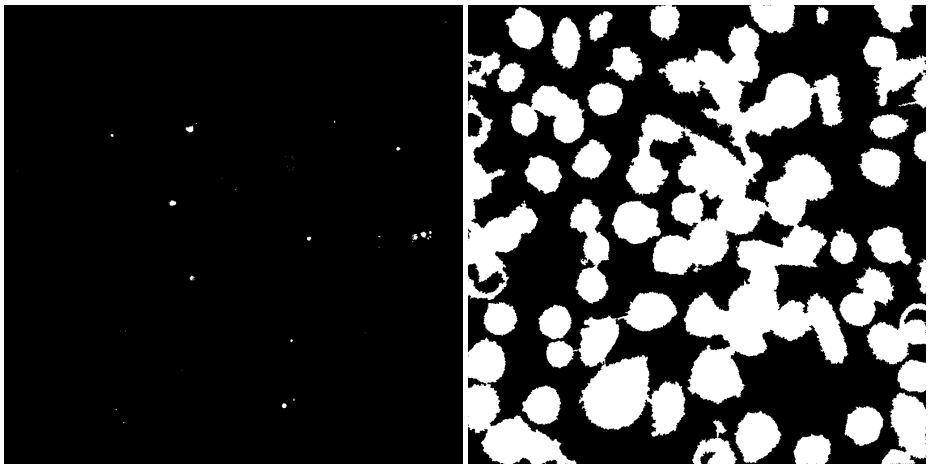

(a) **(b)**

Figure 12: Example of a binary NP stack (a) and cell stack (b) created and used in the MATLAB image analysis script.

4 Results

4.1 Uptake of PIHCA NP/MBs

In the beginning of this thesis, all investigations were qualitative, to ensure that uptake of NPs was taking place. Only after successful uptake of NPs was established were quantitative investigations performed, in order to measure the effect of the treatment. Cellular uptake of NPs after ultrasound treatment was seen immediately in this project, and was in fact seen to some degree in every single experiment.

4.1.1 Qualitative inspection of uptake

Initally, different MIs were tested in order to investigate its effect on cellular uptake. In the successful trials of the project thesis, MIs of 0.47 and 0.65 were applied, indicating that MIs in this range are suitable. Therefore, in the first experiment in this thesis, the following MIs were applied: 0.45, 0.59, 0.85 and 1.12. The highest MI of 1.12 resulted in extensive damage to the cells, and was not used again. Instead, one of the four treatment areas was used for a lower MI of 0.32 in subsequent experiments.

As shown in figure 13, two forms of uptake were seen. The most commonly found form of uptake is shown in figure 13a. In this form, which will be referred to as "simple uptake", one or a few NPs are taken up. These NPs, or aggregates of NPs, are small, and usually separated from each other in the cell. Some cells showed uptake of several NPs, but still the ingested particles were small and far from each other.

The other form of uptake, shown in figure 13b and henceforth termed "clustered uptake", differed from simple uptake in both quantity and appearance. Clustered uptake is characterized by several NPs or aggregates of NPs, often close to each other, and in many cases accompanied by larger aggregates, as shown in figure 13b. Most cells displayed no uptake or simple uptake, while a few displayed clustered uptake. These observations were true for all five MIs (figure 14). While it might seem as though simple uptake and clustered uptake are just varying degrees of the same kind of uptake, the two forms were easily distinguishable. There were also no intermediate form between the two. Each cell that showed uptake, clearly belonged to one of the two categories, and only in very rare cases were there any difficulty placing the uptake seen in the simple uptake or clustered uptake category.

Repeating the experiment, this time with MIs of 0.32, 0.45, 0.59 and 0.85, resulted in the same two forms of uptake, but uptake was seen to a lesser degree in both forms as compared to the former trial. This is likely due to natural variations of the cells from day to day, and/or unintended variations in the amount of MBs/NPs injected into the CLINIcell. Qualitatively, no differences between the different MIs applied could be found.

Images were also taken from untreated areas of the CLINIcells, as shown in figure 14. Some uptake was seen here, but much less than in the treated areas.

The uptake seen in the untreated areas resemble the simple uptake form seen in the areas that received ultrasound treatment.

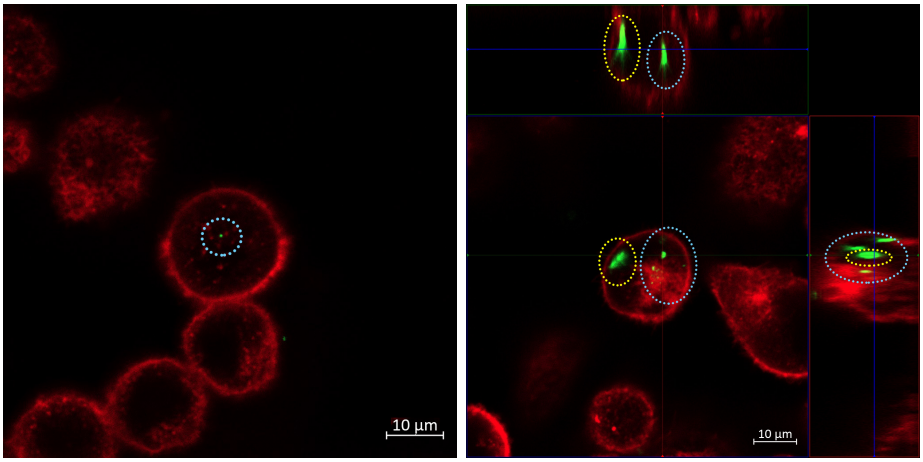

(a) A cell showing simple uptake of a single NP or NP aggregate.

(b) A cell showing clustered uptake (cluster in blue circle) and uptake of a large aggregate (yellow circle).

Figure 13: Two forms of uptake was seen; low uptake (a) and clustered uptake (b). (b) also shows how the imaging software can help determine whether the observed NPs are inside or outside a cell. This is an orthogonal view of the cell, where you get both x-z and y-z views of the cell in addition to the traditional x-y view.

4.1.2 Control sample

To uncover whether the observed uptake was a result of the ultrasound treatment or simply a result of normal endocytosis, a control sample was injected with NPs and MBs, but was not given any ultrasound treatment, ref section 3.4. The results can be seen in figure 15. NP uptake was seen in the control sample as well, showing that normal endocytosis of the NPs by the PC3 cells does occur. The uptake seen in the control sample very much resembles the uptake seen in the untreated areas of treated CLINIcells, with the appearance of simple uptake.

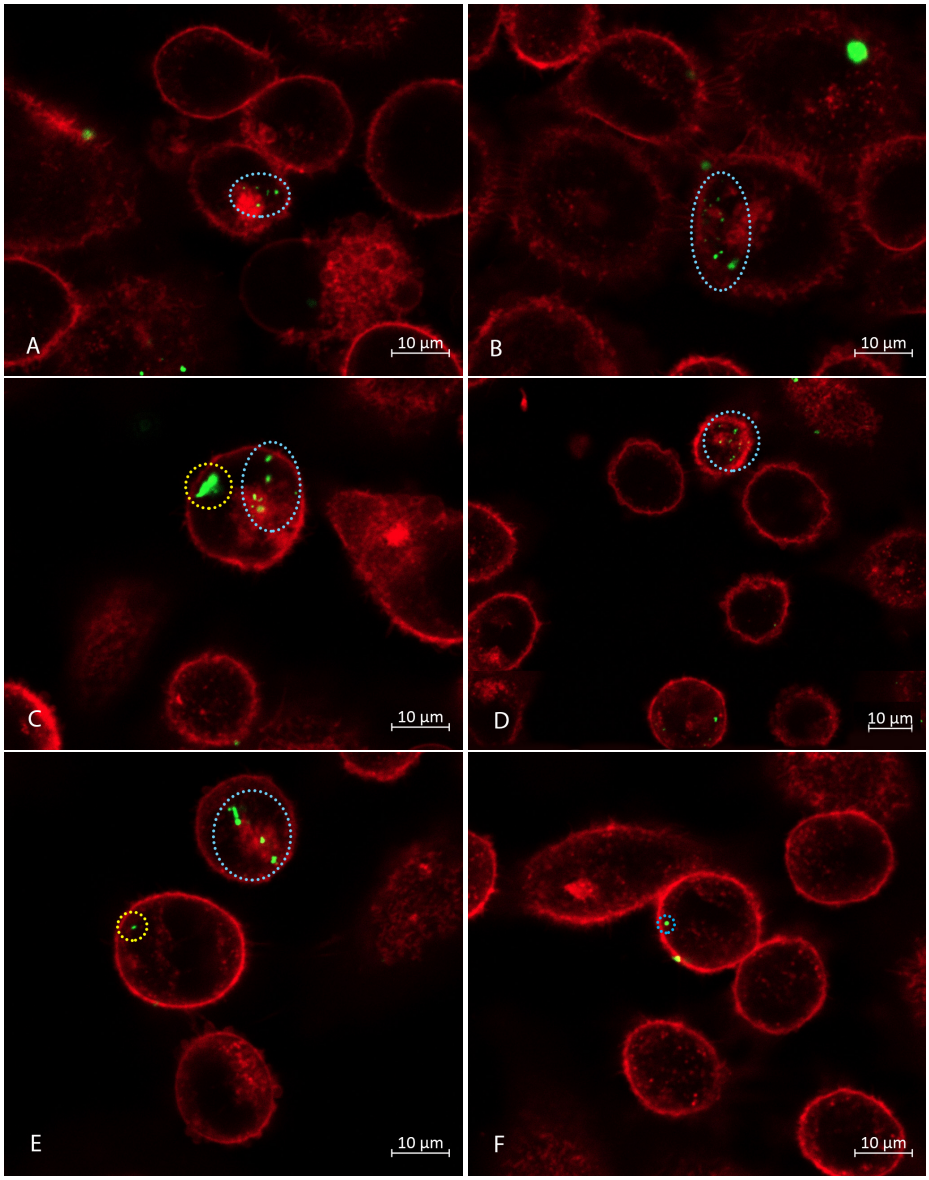

Figure 14: Fig A-E shows clustered uptake after treatment using MIs of 0.32 (A), 0.45 (B), 0.59 (C), 0.85 (D) and 1.12 (E), with 50 Hz PRF and 100 cycles. F shows a typical cell in an untreated control area showing uptake of a single NP aggreagate.

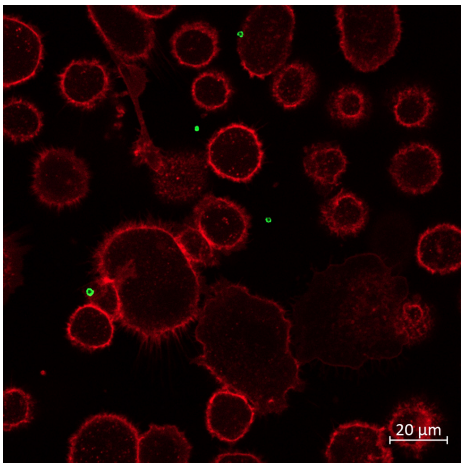

(a) As the sample was not exposed to ultrasound, many MBs are still intact.

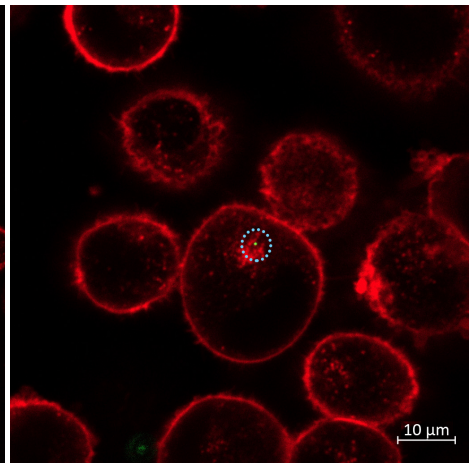

(b) Uptake of a NP or an aggregate of NPs (circled).

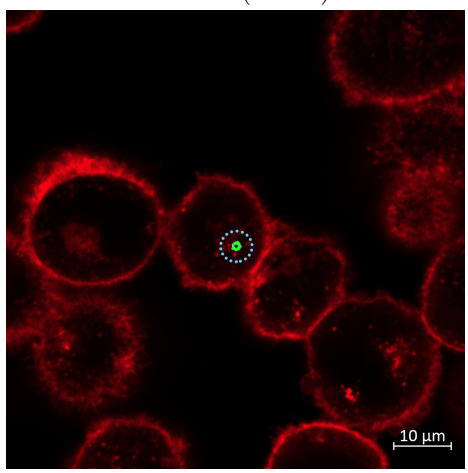

(c) Uptake of an intact MB (circled).

Figure 15: The figure shows three examples of uptake seen in the control sample, which was not exposed to ultrasound. Most cells showed no uptake (a), while some cells showed uptake resembling simple uptake (b). As no ultrasound was used on this sample, some MBs are still intact (a and c), and could even be taken up by cells (c).

4.1.3 Quantitative inspection of uptake

Because uptake was seen in the absence of ultrasound, a more quantitative analysis was needed in order to establish the effect of the ultrasound treatment. Quantitative inspection and analysis was done as described in section 3.9. Examples of the images that were obtained and subsequently analyzed are shown in figure 16.

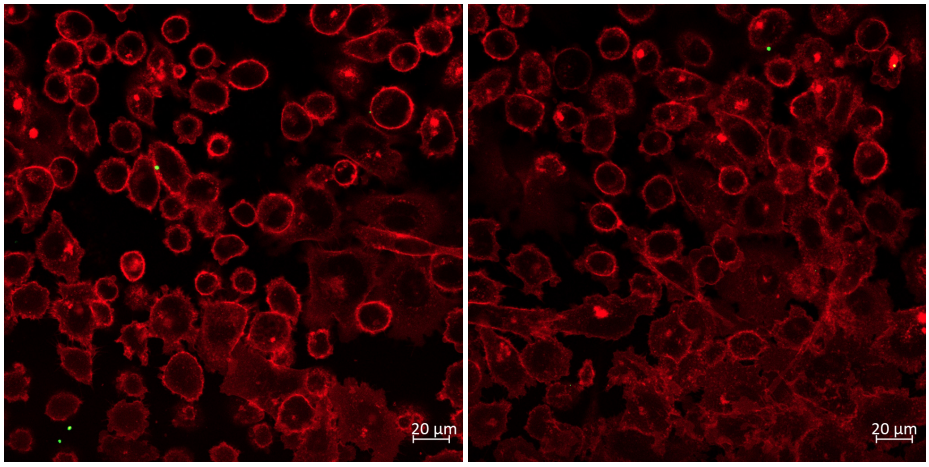

(a) Example of an overview image from a treated area (0.59 MI).

(b) Example image of an untreated control area.

Figure 16: Examples of images that were obtained and subsequently analysed during quantitative analysis of the effect of ultrasound treatment, as described in section 3.9.

Different MIs were applied to uncover the influence of acoustic pressure on the resulting uptake. The applied MIs were 0.32, 0.45, 0.59 and 0.85, and the experiment was performed twice. The results are shown in figure 17. As there was more than twice as much uptake for the two lower MIs (0.32 and 0.45) in the first trial compared to the second, the two trials are also shown independently (figures 17a and 17b). Quantitative analysis revealed that, averaging the two trials, each of the four treatments resulted in a significant increase in cellular uptake as compared to untreated control cells (figure 17). Additionally, the 0.59 MI treatment resulted in significantly higher uptake compared to the two lower MIs. However, because of the large variations between the two trials, it would be premature to conclude that there is a trend of increasing uptake with increasing MI.

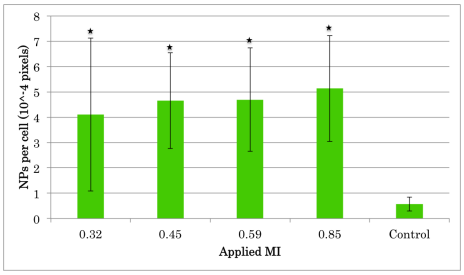

(a) Trial 1 (n=8-9).

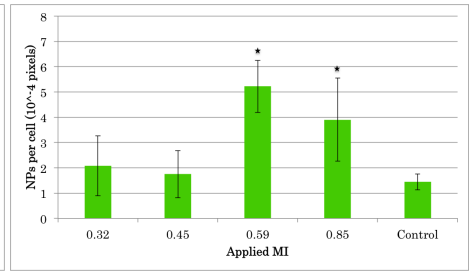

(b) Trial 2 (n=8-9).

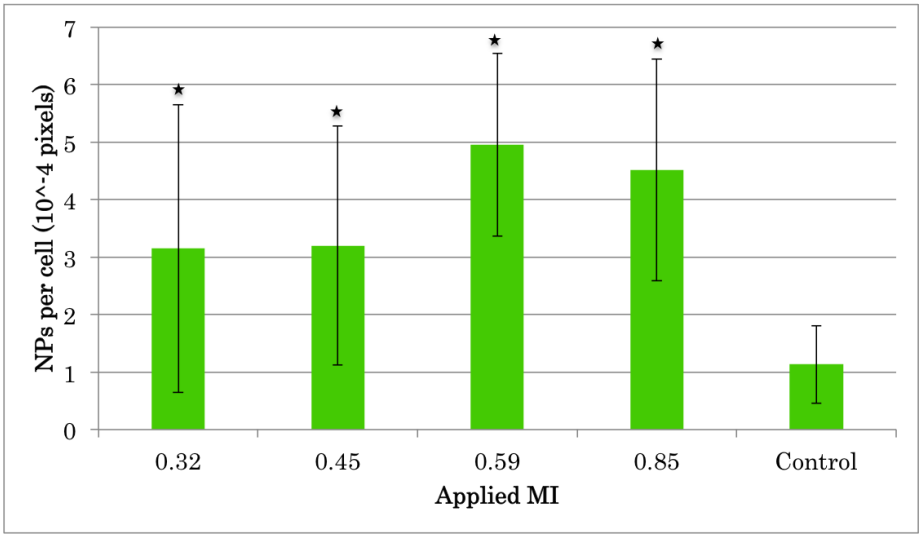

(c) Average of the two trials, with SD calculated from all (n=17-18) images from each MI treatment.

Figure 17: Results from the investigations of the effect of MI on cellular uptake. The values shown are the average amount of NP pixels per cell pixel, and the standard deviations are based on all images from the given treatment area. The results show no significant increase in uptake with increasing MI for the first trial (a), while in the second trial (b) the two higher MIs are significantly higher than the two low MIs. In the first trial all MIs lead to a significantly higher uptake, while in trial 2 this is only true for the two high MI treatments. Averaging the two trials (c) shows that each MI leaad to a significantly higher uptake than the control, with the increase being the highest for the 0.59 and 0.85 MI.

Lower MIs of 0.1 and 0.2 were tested against 0.45 and 0.59 in order to see whether the uptake is different when the MBs show stable cavitation (as with lower MIs of 0.1 and 0.2) compared to when there is MB destruction and possible inertial cavitation (higher MIs of 0.45 and 0.59). The experiment was performed twice, and the result are presented in figure 18. The results from the two trials differed a lot, and are therefore presented separately (note the differences in the two y-axes). In both trials, the lowest MI produced the lowest increase in uptake, and in neither experiment was this increase significantly higher than the control. The other three MIs lead to significantly higher uptake than the control in both trials. There seems to be a clear increase in uptake as the MI is increased above 0.1, but above this, the uptake does not increase with increasing MI. Figure 19 shows the amount of NPs colocalized with cell membranes after ultrasound treatment, showing a significantly higher amount of colocalized NPs for the 0.2 MI treatment compared to the two higher MIs as well as the control. Also the 0.1 MI treatment leads to more colocalized NPs than the two high MI treatments. Comparing the aggregates seen in these low MI areas to the ones seen in higher MI areas, it seems that the aggregates resulting from the low MI treatments are both larger, more spherical, and more numerous.

A cycle length of 100 cycles and a PRF of 50 Hz was used in all experiments until this point. In order to see the effect of varying the cycle length and PRF, and thus also the duty cycle (DC), two areas of a CLINIcell were treated with 100 cycles and 50 Hz PRF and the remaining two with 1000 cycles and 100 Hz PRF, with two different MIs for each cycle setting, 0.3 and 0.59 (section 4.1.3). The experiment was performed twice. Because of considerable differences between the two trials, results from the two trials are presented serparately in figure 20.

Table 2: Overview of the four treatment areas and their respective ultrasound settings when investigating the effect of pulse length and PRF on cellular uptake.

Treatment area	MI	PRF	Cycles
1	0.3	50	100
2	0.3	100	1000
3	0.59	50	100
4	0.59	100	1000

All four treatments lead to a significant increase in uptake with respect to the control in at least one of the two trials. Again there does not seem to be any trend of increasing uptake with increasing MI, nor is there any clear differences between the different MIs. This is also clear from the representation of the average of the two trials, which shows a significant increase in uptake for all four treatment with respect to the control, as well as no significant increase in uptake with increasing MI. There is however, on average, a significant increase in

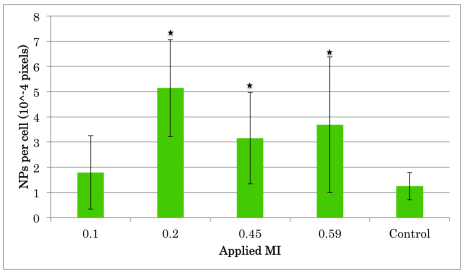

(a) Trial 1 (n=9 for treated areas, n=5 for control).

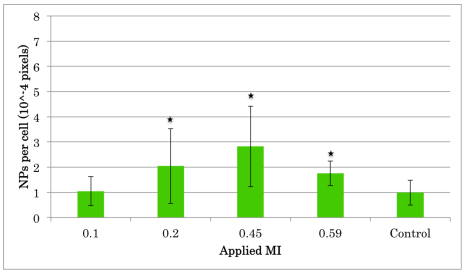

(b) Trial 2 (n=9 for treated areas, n=6 for control).

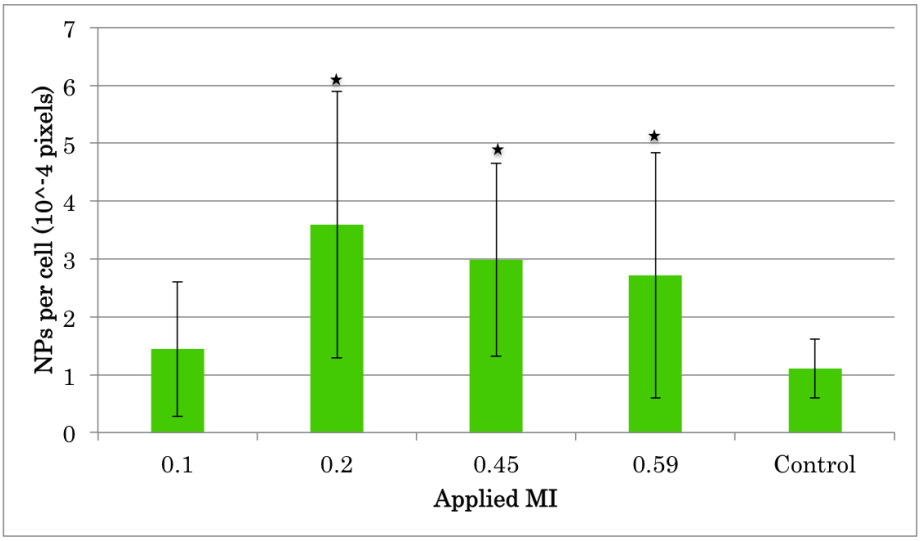

(c) Average of the two trials, with SD calculated from all (n=18 for treated, n=11 for control) images from each MI treatment.

Figure 18: The figure shows the effect of high and low MIs on cellular uptake of NPs. The 0.1 MI treatment leads to only a slight increase in uptake, while MIs of 0.2, 0.45 and 0.59 all lead to significantly increased uptake compared to the control. In both trials (a) and (b) and for the average of the two (c) there is a clear increase in uptake as the MI is increased from 0.1 to 0.2. Above this MI however, there is no clear trend of increasing uptake with increasing MI.

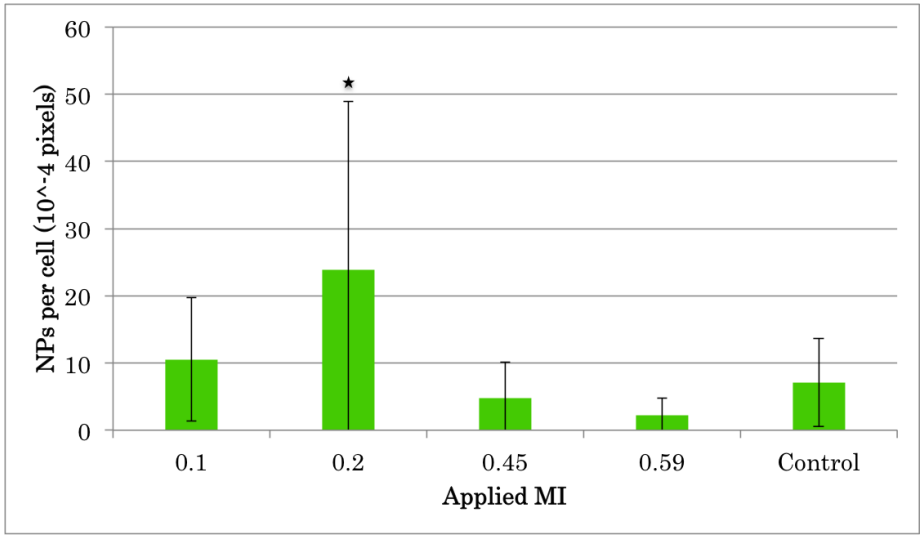

(a) Figure showing the amount of colocalized NPs after ultrasound treatment. Averages and standard deviations are calculated from all n=18 trials (n=11 for control).

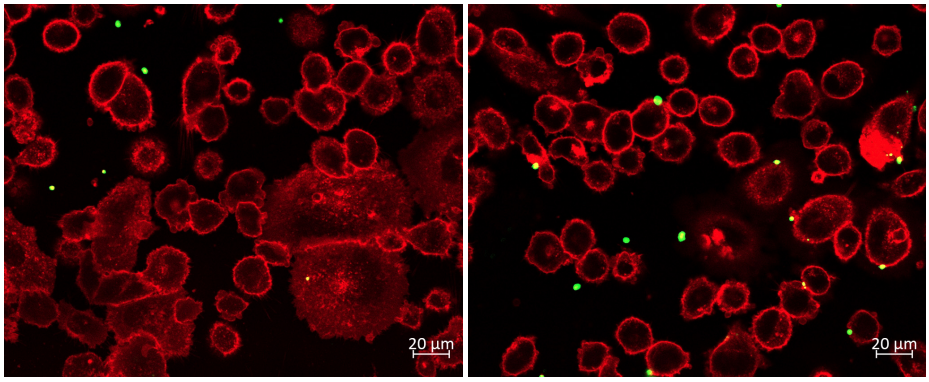

(b) **(c)**

Figure 19: Colocalization of NPs after ultrasound treatment is higher when using low MIs, and the 0.2 MI treatment in particular is significantly higher than both the control, and the two higher MI treatments (0.45 and 0.59) (a). (b) and (c) shows examples of images analysed from the 0.1 and 0.2 MI treatment, respectively. Comparing these images to figure 16(a) one can see that the aggregates obtained after applying lower MIs, in particular 0.2 MI, are both larger and more numerous.

uptake with increasing pulse length and PRF, which is also shown in figure 21a.

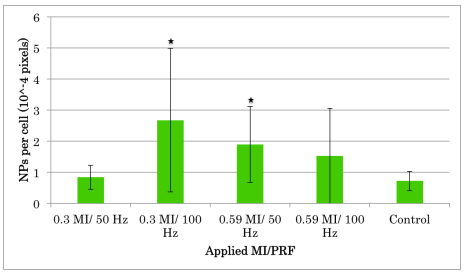

(a) Trial 1 (n=8-9).

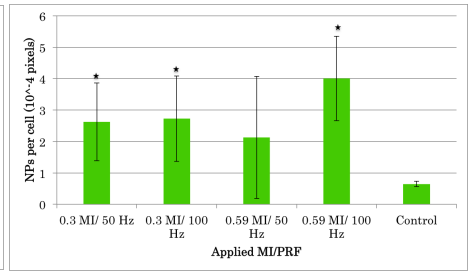

(b) Trial 2 (n=8-9).

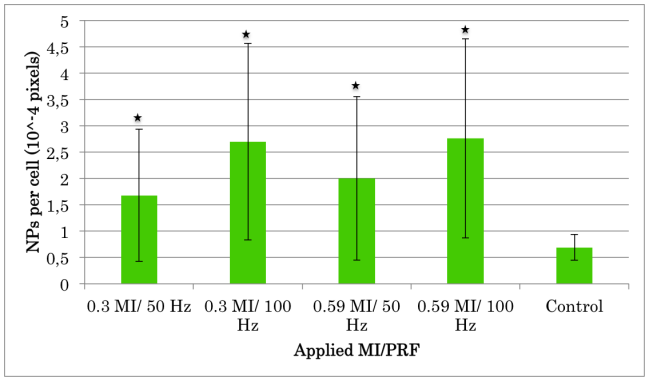

(c) Figure shows the average of the two trials (n=17-18).

Figure 20: The figures show the results from two identical experiments where varying PRFs and pulse lengths were applied. Averages and SD were calculated from all analysed images from each treatment.

When looking at the amount of NPs localized with cell membranes, a massive difference between the two duty cycle settings is revealed (figure 21b). Averageing the two trials, the treatments with 100 Hz PRF and long pulses lead to more than an eight-fold increase in NPs found on cell membranes, compared to using shorter pulses and a lower PRF.

If comparing the applied MIs for all areas treated with 100 Hz and 1000 cycles, there is significantly more NPs co-localized with cell membranes for 0.3 MI than for 0.59 MI. Moreover, cells treated with the high MI and high duty cycle, do not show a significant increase in colocalized NPs compared to untreated cells (figure 21c). Examples of images from areas treated with 1000 cycles and 100 Hz PRF are shown in figure 22. The aggregates seen after treatment with this high duty cycle are, as when treating with low MIs (figure 19) larger and more numerous than when treating with a lower duty cycle. Figure 21d shows a comparison of the amount of colocalized NPs between using a high duty cycle and using low MIs. The higher duty cycle treatment

leads to more than twice as much colocalized NPs, a significant difference. This is in accordance with the images (figures 19 and 22), from which it seems that the aggregates formed during the high duty cycle treatment are more consistently assosiated with cell membranes, whereas the aggregates formed during low MI treatment seem to be more randomly distributed around the treated area.

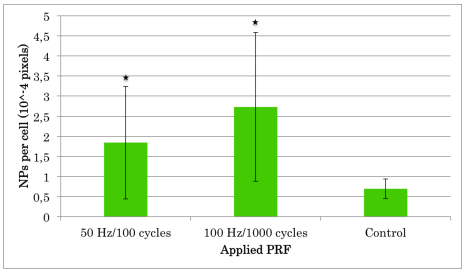

(a) Amount of uptake as a function of applied PRF and cycle length (n=34; n=13 for control).

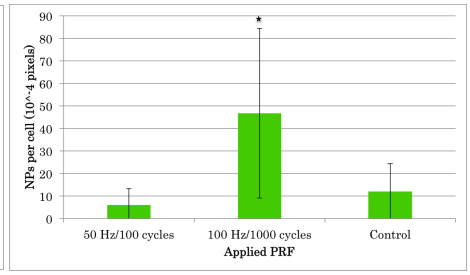

(b) Amount of NPs colocalized with cell membranes as a function of applied PRF and cycle length (n=34; n=13 for control).

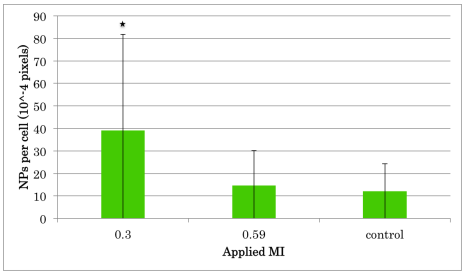

(c) Colocalized NPs after treatment with 100 Hz PRF and 1000 cycles pulse length, as a function of applied MI (n=34; n=13 for control).

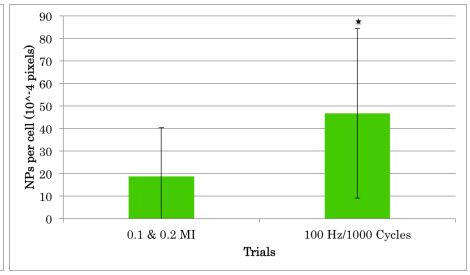

(d) A comparison of the amount of colocalization when treating with low MIs and when treating with high duty cycles (n=34-36).

Figure 21: The figure shows the effect of varying the PRF and pulse length of the treatment. Averages and SD calculated from all analysed images from each treatment.

Next, ultrasound treatment was performed at 4°C in order to avoid normal endocytosis of the PIHCA NPs. The results are shown in figure 23. Note that only the treatment was performed at 4°C, not the imaging. The temperature in the CLINIcell therefore increased during the course of imaging, and with it, the amount of normal endocytosis likely increased. The imaging was done in order of increasing MI, ending with the control. All treatments resulted in uptake of NPs, and for all but the 0.32 MI treatment, this uptake was significantly higher than the control.

To better understand what happens in the hours after ultrasound treatment, one particular area of the sample was imaged shortly after treatment, and again roughly three and a half hours later. This is shown in figure 24. A cell showing a relatively high amount of NPs on its cell membrane shortly after treatment is

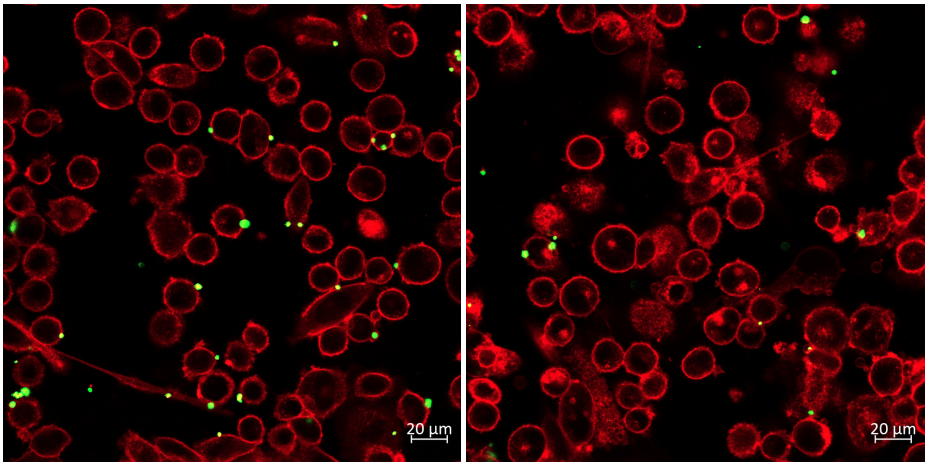

(a) **(b)**

Figure 22: Examples of images from the areas treated with (a) 0.3 MI and 100 Hz, and (b) 0.59 MI and 100 Hz, showing a high amount of large NP aggregates. This is especially prominent in (a).

circled in blue. During the course of almost four hours, there seems to be little or no uptake of these NP aggregates.

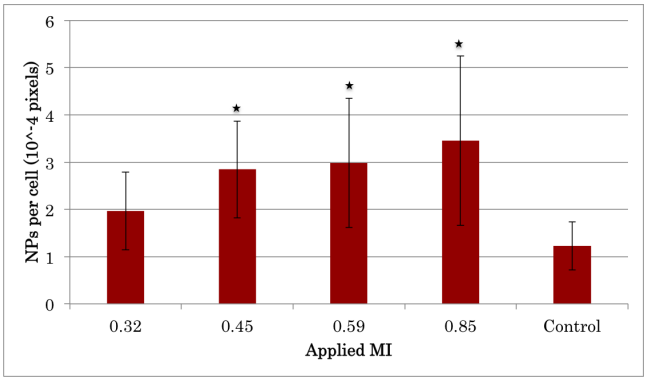

Figure 23: The figure shows the cellular uptake of PIHCA-stabilized NPs for each treatment at 4°C, and for untreated areas. Averages and SD calculated from all analysed images from each treatment (n=8-9).

4.2 Uptake of NPs after co-incubation

An important part of this project was to investigate the effect of the PIHCA-stabilized MBs versus commercial MBs such as Sonazoid. First, qualitative inspection of the result after ultrasound treatment was performed in order to

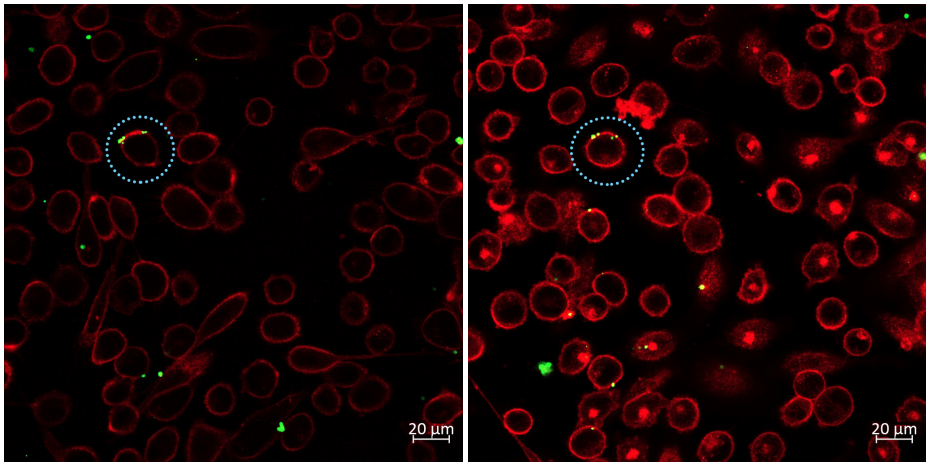

(a) **(b)**

Figure 24: Images of the same area of the sample (a) shortly after treatment with PIHCA-stabilized NPs at 4°C, and (b) roughly three and a half hours later. Despite NPs being seemingly embedded in the cellular membrane in (a), no or very little uptake of these NPs was seen in the following hours.

investigate whether there were any qualitative differences in the type of uptake as compared to the treatments using the PIHCA-stabilized MBs. Next, the experiment was repeated twice and quantitative analysis of the result was performed. As can be seen from figure 25, NPs was again observed inside cells after treatment. However, the amount of uptake seemed to be somewhere between untreated cells and cells treated with ultrasound in combination with PIHCA-stabilized MBs. Clustered uptake was found after co-incubation, but not as frequently or intense as in the previous trials (figure 14).

The quantitative results shown in figure 26 shows that the use of Sonazoid MBs does in fact lead to a significant increase in uptake compared to untreated cells. However, as shown in figures 27 and 28, this increase is significantly lower than when using the PIHCA-stabilized MBs, for all four MIs. Additionally, even treating with PIHCA-stabilized MBs at 4°C leads to significantly higher uptake than with co-incubation, for all MIs but one (0.32 MI).

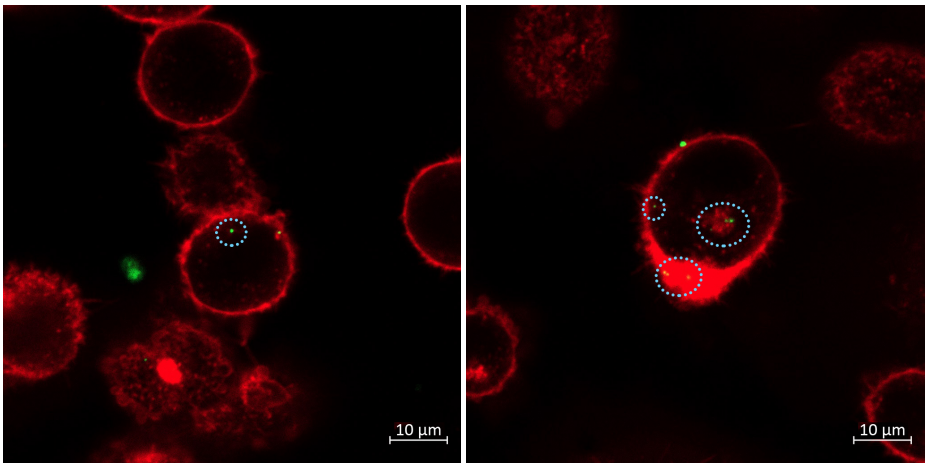

(a) Uptake of a single NP or NP aggregate after treatment with 0.32 MI.

(b) Uptake of NPs, resembling a modest form of clustered uptake after treatment with 0.59 MI.

Figure 25: Figure demonstrating the uptake seen after co-incubation of Sonazoid MBs and free NPs.

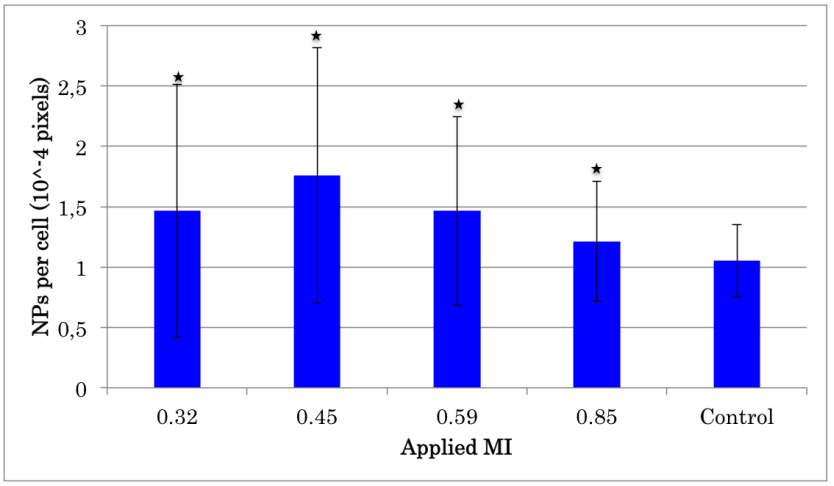

Figure 26: Averaged uptake of the two trials using co-incubation of NPs and commercial MBs. Averages and SD calculated from all analysed images for each MI and control (n=18).

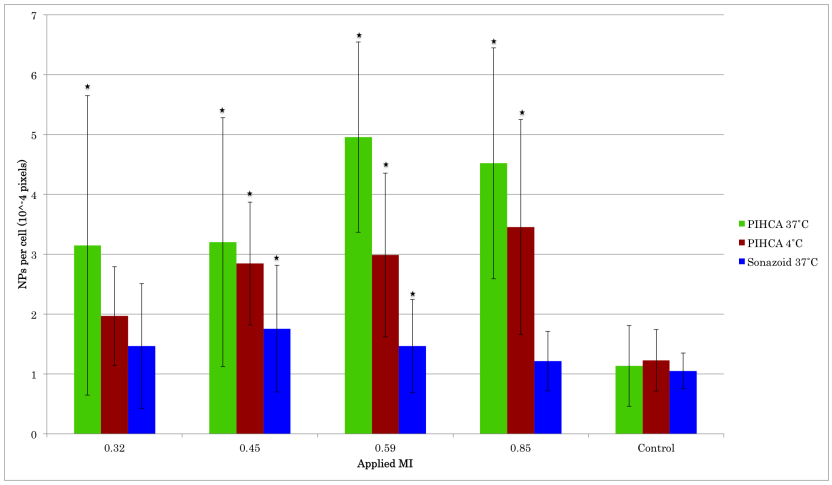

Figure 27: A comparison of cellular uptake after ultrasound treatment using PIHCA stabilized MBs at 37°C (green), at 4°C (red) and commercial Sonazoid MBs 37°C (blue). Averages and SD are calculated from all analysed images from each treatment. (n=17-18 for PIHCA 37°C and Sonazoid 37°C; n=8-9 for PIHCA 4°C)

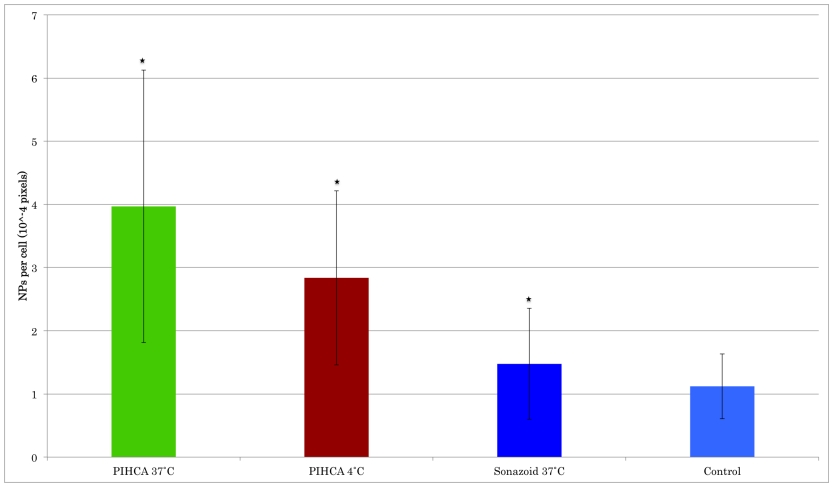

Figure 28: A comparison of cellular uptake, showing an average of all four treated areas, between PIHCA stabilized MBs at 37°C, at 4°C and commercial Sonazoid MBs at 37°C. Averages and SD are calculated from all analysed images from each experiment (n=71-72 for PIHCA 37°C and Sonazoid 37°C; n=34 for PIHCA 4°C). Average and SD for the control in this figure are calculated from all three experiments (n=44).

5 Discussion

5.1 Cellular uptake of NPs after ultrasound treatment

The results presented in this thesis show that ultrasound treatment in combination with PIHCA-stabilized MBs can lead to an increased cellular uptake of PIHCA NPs. Cellular uptake following ultrasound treatment was seen in two forms; clustered uptake and simple uptake. The two forms might result from two different uptake mechanisms, or they could be a result of varying degrees of the same uptake mechanism. Considering that most of the cases of clustered uptake were so easily distinguishable from simple uptake, with no intermediary forms, the former seems the most likely explanation. From a purely intuitive perspective the clustered uptake seems like what one might expect to see if a pore in the cell membrane was opened for a brief duration, and an excess of NPs were allowed to rush into the cell before the pore closes. In addition, it is easy to imagine how the appearance of the simple uptake can be the result of one or several endocytosis events.

As described in section 2.7.3, cavitation of MBs can be either stable, or inertial. This is an important distinction because the two cavitation modes can lead to different biophysical responses in the cell. This can mean a different size-range of pores created, or a different uptake mechanism alltogether. The two main uptake mechanisms that are of relevance to this discussion are sonoporation and enhanced endocytosis. Which of these uptake mechanisms are involved will depend on the behaviour of the MBs during ultrasound exposure, which in turn depends on MB size, MB shell composition, and applied MI. It is therefore important to uncover the behaviour and destruction of the NP-stabilized MBs in response to different acoustic pressures.

The initial hypothesis was that the NPs, due to their size (177 nm diameter), can only enter via rather large pores, created after collapse of an inertially cavitating MB. The uptake should therefore be significantly higher for high MIs than for low MIs, which do not lead to inertial cavitation. However, if ultrasound-induced endocytosis is the most important mechanism for cellular uptake of PIHCA NPs, the picture will be different. In that case the difference between various MIs could be insignificant, or the lower MIs could even produce more uptake since fewer MBs will undergo inertial cavitation, leaving more MBs to undergo stable cavitation which leads to enhanced endocytosis. Additionally, it was expected that the higher the MI, the bigger and longer lasting the pores through wich more NPs could enter. It was therefore expected to see an increase in uptake with increasing MI.

Considering the many papers supporting the theory that increasing acoustic pressures lead to a larger MB response and larger pores in the cell membranes [42, 43, 44, 45, 26], the fact that no such trend was seen in this experiment was unexpected. A large variety of ultrasound parameters were used in these papers, with a wide range of acoustic pressures, frequencies and treatment times. Despite these differences, all report seeing a trend of increasing pore size and uptake with increasing MI. Thus, the most likely explanation as to why the

results in this report deviates so much from those papers, seems to be the NP-stabilized MBs used.

The unique new aspect of this thesis is the MBs. The other papers referenced to in this discussion did not use a NP-stabilized MB, but rather a variety of commercial MBs. These MBs often have a lipid or protein shell which might respond differently to ultrasound than the MBs used here. Lipid shelled MBs in particular are more flexible than protein or polymer shells, and will undergo oscillations at lower pressures [27]. Hard shelled MBs on the other hand will not respond so willingly to the applied ultrasound and could even remain unaffected at lower pressures [28]. Polymer shells seem to be the most rigid type, while protein shells lie somewhere between lipids and polymers [27]. Considering that the MBs used in this project consist of a shell of NPs composed of PIHCA polymers, it could seem reasonable to assume that these MBs will behave like hard-shelled MBs rather than flexible MBs. On the other hand, the NP shell consists of independent NPs which could to some degree move independently of each other, potentially leading to a higher degree of flexibility. Indeed, characterization of these MBs shows that they respond with stable oscillations at MIs as low as 0.1 (unpublished results), which more resembles lipid MB behaviour rather than hard-shelled MBs. It is even possible that the MBs are as flexible as lipid MBs, but as robust as hard-shelled MBs, leading to a hybrid behaviour. In short, the NP-stablized MBs' behaviour is important to understand, but difficult to predict.

If the NP-stablized MBs behave as hard-shelled MBs, they might give rise to a binary situation in which the MBs either create a very strong response through sonic cracking if the MI is high enough or no response at all. It is not clear whether the crack and subsequent gas escape during sonic cracking is directed towards a nearby cell membrane - such as the jet created after inertial cavitation of softer MBs - or if the cracking direction is arbitrary. If it is not necessarily directed towards nearby cells, the likelyhood of a cell being punctured decreases, which could explain why clustered uptake was not seen to a greater extent. Sonic cracking could also explains why there were no visible differences in uptake with increasing MI above a treshold of 0.2 MI. However, it is unlikely that an MI of 0.2 is enough to induce sonic cracking of the MBs, and characterization of the MBs has, as mentioned, shown that the bubbles oscillate at even lower MIs than 0.2. The sonic cracking theory is also not in agreement with Bouakaz et al. who defines a nondestruction zone below MIs of 0.3. Over this MI, they conclude, destruction can take place, depending on, amongst other things, MB size [28]. They did however use a double polymer/albumin walled MB, which could potenitally be even stiffer than the MBs used here. The destruction zone in our experiment might therefore begin at MIs lower than 0.3. Even if the NP-stabilized MBs should be viewed as flexible, oscillating at low MIs, the manner in which they collapse can still resemble that of hard-shelled MBs, with a treshold as just described.

Comparing low and high MIs (**??**) there seems to be a clear difference in uptake between the lowest MI of 0.1, and the rest of the treatments. This indi-

cate that the treshold for sonoporation lies somewhere between 0.1 and 0.2 MI. There is a slight increase in uptake even for 0.1 MI, which could be attributed either to enhanced endocytosis by stable cavitation, or to sonoporation after destruction of very few MBs. Considering the low pressure, the former seems like the most likely explanation. The clear differences between 0.1 MI and the higher MIs indicate that sonoporation is a more important uptake mechanism than enhanced endocytosis. Moreover, the fact that the uptake is so high for 0.2 MI, and does not increase further indicates two things. First, that stable cavitation might play a more important role than expected, and secondly, that there is a threshold above which the sonoporation creates large enough pores for the NPs to enter.

It should be noted that further study of the images taken from the low MI areas, especially 0.2 MI, reveal that the measured uptake might in fact be artificially high. One thing that becomes clear from the images of the 0.1 and 0.2 areas is that the treatment leads to the formation of large aggregates of NPs or MBs, possibly due to Bjerknes forces [26]. These aggregates are often locaten near or on a cell membrane. Because of inaccuracies in the analysis tools, and/or bleed-through of the NP signal into z-planes where there really are no signal, parts of these aggregates are being counted as internalized NPs. This means that the uptake for 0.1 and 0.2 MI shown in figure 18 is slightly high. From the images it does seem like there is an uptake at 0.2 MI though, and it is not likely that all the uptake seen is due to artefacts in the image. **??** shows that the uptake at 0.2 MI is actually higher than both 0.45 and 0.59 MI. It is possible that the three MIs really lead to the same amount of uptake, or that there should be a more stepwise increase in uptake between 0.1 MI and the two highest MIs. This would be more in accordance with the litterature, with increasing MI leading to larger and longer lasting pores, through which more NPs could potentially get in. The aforementioned aggregates can have a negative effect on uptake as they are, in many cases, far too large to enter the cells via pores. However, assuming that the aggregates are mainly composed from free NPs, and cellular uptake is mainly of NPs from the MB shell, this does not necessarily impact the results.

Another aspect to consider is that the MBs might break up into pieces after collapse. These pieces might subsequently be endocytosed by the cell due to enhanced endocytosis or they can be taken up through newly created pores. Ibsen et al. reports that the higher the MI, the smaller the fragments of the MB shell [46]. That study involved lipid shells, but it is possible that the same behaviour is true for our MBs. On the other hand, Bloch et al. reports that the hard polymer shell of their MBs remains intact after the gas escapes it [27]. Since our results show no clear differences between the different MIs used, that could mean that the MB shell does not break into pieces following gas escape from the MBs. During imaging, however, no intact MBs were seen in areas treated with MIs of 0.32 or higher. Additionally, because uptake was seen after stable cavitation (0.2 MI), and because stable cavitation pushes free NPs away from the MB [37], it seems that the NPs taken up are the NPs initially

comprising the MB shell. It therefore seems that the MB shell does break up. Because the MB shell is made up of individual NPs, it is possible that the shell fragments are largely independent of MI. If so, it seems that an MI of 0.2 is required to create pores large enough for entry of these fragments, as no significant increase in uptake compared to the control was seen below this MI.

The fact that uptake is seen even during stable cavitation is an important point in this thesis. The idea behind NP-stabilized MBs is that the NPs should be as close as possible to the cell membrane pore being created by the cavitation. When the MB is destroyed, the NPs that made up the shell can enter the cell through the nearby pore. The reason for this design is as mentioned that during stable cavitation the cavitating MB will push free NPs away from it and the cell. When the pore then opens, no NPs are in the vicinity of it, and no entry of NPs occurs. The fact that uptake is seen after stable cavitation indicates that the design of the NP-stabilized MBs work, and that the NPs from the MB shell enter the cell. This also presents a possible explanation as to why the uptake does not increase with increasing MIs above 0.2. If the NPs that are taken up are the ones that comprised the MB shell, only these NPs are able to enter the cell, regardless of the applied acoustic pressure.

The discussion so far has focused on sonoporation rather than enhanced endocytosis. The results from the treatment at 4°C supports the hypothesis that sonoporation is the dominant uptake mechanism. As figure 23 shows, uptake was seen even when treating the sample at 4°C, where presumably no enhanced endocytosis could take place. There also seems to be a trend of increasing uptake with increasing MI. Because the cells are not chemically fixated, and because imaging happens at room temperature (RT), treating the sample at 4°C will only stop endocytosis during treatment, and not during imaging, as the temperature in the CLINIcell slowly increases to RT. Also, not all of the free NPs in the MB solution that is being injected into the CLINIcell during treatment will be washed out of the CLINIcell when the medium is removed, and will thus stay on or near the cells. When the temperature increases during imaging, these NPs can eventually be ingested by the cells. As the imaging was performed in order of increasing MI, ending with the control cells, the trend seen might infact only be increasing amount of normal endocytosis over time as the temperature increases (see **??** for details on imaging duration and time between imaging of different treatment areas). As the control areas were imaged last (after a few hours), this explains why the uptake seen in the control areas are similar to what was seen in previous experiments. The relatively high uptake seen in the 0.32 MI treatment, when the temperature was presumably still low enough to inhibit endocytosis, shows that ultrasound-induced uptake via pore formation does occur during treatment. Comparing the results from the 0.32 treatment at 4°C and 37°C (figure 17), the amount of uptake is almost the same. The difference in uptake between these two treatments is about the same as the amount of uptake seen in the control areas. This indicated that the difference between the two experiments (4°C and 37°C) is due to normal endocytosis, which further shows that enhanced endocytosis plays an insignificant role in the

uptake of the NPs, and that entry through pores is the dominant mechanism.

Another approach to stopping endocytosis in cells, is by addition of endocytosis inhibitors. Afadzi et al. saw that, although complete inhibition of endocytosis did not completely block cellular uptake - proving that sonoporation plays a role - endocytosis plays an important role [42]. Meijering et al., also by using endocytosis inhibitors, came to a similar conclusion, with endocytosis playing a key role in ultrasound mediated uptake [34]. Interestingly they concluded that smaller molecules are more likely to enter cells through pores, while larger molecules are mainly endocytosed. As the NPs used in our project are rather large in this context, this should mean that the NPs would be taken up mainly by endocytosis. However, both those studies differ from this one both in uptake agents and MBs (they used dextrans and commercial, lipid shelled MBs). It is in general important to keep in mind the differences in both MBs and uptake agents between those studies and this one, and that such results are hard to translate between different studies. If anything, the comparison between their results and the results seen here after ultrasound treatment at 4°C, further proves how important the MB composition and uptake agent size is in this equation.

On the topic of sonoporation versus enhanced endocytosis, an imporant aspect has been left out, namely the interrelation between the two mechanisms. It has been shown that endocytic activity in cells increases after cellular damage, such as pore formations, as a repair mechanism to remove the pores [47]. The response of the MBs depends on an interplay between applied MI, MB size [48] and MB composition [26]. It is therefore possible that, due to the large polydispersity of the NP-stabilized MBs used, the response to the treatment varies across a sample during treatment, leading to both stable and inertial responses and a large variety of pore sizes. If the pores created are too small for the PIHCA NPs to enter, they can still induce a repair mechanism in the form of endocytosis and NPs could still be taken up by cells. On the other hand, if inertial cavitation results in pores big enough for the NPs to enter, the effect could be further enhanced by the following endocytosis. This could explain the big differences seen between clustered uptake cells and simple uptake cells, where a pore size threshold is created above and below which clustered and simple uptake is seen, respectively.

The big difference in uptake between clustered uptake and simple uptake is reflected in the large standard deviations seen in almost every plot in the results of this report. Because some cells will be completely without uptake of any kind, and some cells will show clustered uptake, even though the *average* uptake is only slightly higher than the control, the standard deviation will be very high. This is also why the standard deviation in the control areas are comparatively small in every experiment. Moreover, the standard deviation can actually help indicate how the cells have been affected by the ultrasound treatment. For example, the standard deviation gives yet another indication that the cells treated with 0.1 MI has not been affected in the same manner as cells in the other treatment areas, as its standard deviation bar is considerably

smaller than the others, and looks more like the standard deviation of the uptake in the control area.

Another possibility is that only clustered uptake is a result of sonoporation, while simple uptake is a result of normal endocytosis by the cells. Simple uptake was in fact observed in untreated control areas of the treated CLINIcells, but there was a concern that the uptake seen in these untreated areas was a result of the ultrasound treatment. The pressure profile of the 1 MHz ultrasound transducer is quite steep **??**, and outside a radius of about 5 mm around the center of the exposed area the ultrasound treatment should have virtually no effect. However, because of the possibility that treated cells could migrate away from the treated area and into the untreated areas, the control sample was prepared as described in **??**. After the control experiment (with no ultrasound exposure) it was clear that some uptake did take place even in the absence of treatment. The uptake seen in the control experiment, shown in figure 15, is likely due to normal endocytosis of the PC3 cells, as described in section 2.5. Also, the uptake seen in the control sample greatly resembles uptake found in the untreated areas of samples exposed to ultrasound, both in terms of amount and appearance of uptake. It therefore seems that the untreated areas of each treated CLINIcell can indeed act as a reliable control.

Both the control sample and the control areas of treated samples displayed simple uptake of NPs. Although there was occationally cells showing more uptake than usual for control cells, no clustered uptake was seen in untreated cells at any time during this thesis. It therefore seems that uptake resulting from normal endocytosis will generally have the appearance of varying degrees of simple uptake. Additionally, normal endocytosis will naturally occur all across the sample, also in treated cells. This is why there is a possibility that the simple uptake seen in treated areas is a result of normal endocytosis, and not a result of sonoporation. However, distinguishing between ultrasound-dependent and -independent endocytosis, especially if the effect of the ultrasound is small, might be difficult, at least qualitatively.

5.2 Confluency of cell layer in CLINIcell during treatment

Achieving the optimal amount of cells on the day of treatment is challenging. Few cells means fewer chances of achieving sonoporation, while excess cells can be detrimental in its own way. When the cells in an area reaches confluency, but continues to divide, the new cells lie on top of the original cell layer, loosely attached to it. These extra cells might receive the effect the ultrasound treatment, only to be subsequently washed away when removing the medium. This could make it impossible to evaluate the effect of the treatment. Because too few cells could cause even bigger problems than having slightly too many cell, the amount of cells were usually kept "on the safe side", meaning that a bit more than the ideal amount of cells was seeded in each CLINIcell. It is possible that this could explain some of the difference between identical experiments, for example like the ones seen in figure 17a and figure 17b.

Even if the ideal amount of cells are achieved before treatment, other chal-

lenges arise that might make the analysis of the results difficult. One such challenge is that the cells can detach from the CLINIcell membrane. Ultrasound treatment is shown to lead to disruptions of the cellular structural integrity, not only in terms of the cell membrane, but also the cytoskeleton, thereby weakening the attachment of the cells to the growth substrate [49, 50]. Cells that have been exposed to ultrasound are thus especially vulnerable to being washed away when changing solutions during treatment. Even prior to ultrasound treatment there were non-confluent areas in nearly every CLINIcell. The confluency problem seemed to be more prominent near the two inlets of the CLINIcell, possibly because of injection and ejection of solutions that affect the adhesion of cells to the CLINIcell membrane in these areas.

5.3 Effect of cycle length and PRF on cellular uptake

Cycle length and PRF, related by the duty cycle, can greatly affect the biophysical effect of ultrasound treatment. As with most things in the field of sonoporation the exact dependency on these factors will vary between different types of bubbles. Fan et al. found that short pulses resulted in high cell viability and high delivery rates, while long pulses resulted in translational movement of the MBs leading to massive cell death because of cell membrane disruptions [51]. Zhou et al. similarly found that longer pulses lead to higher acoustic radiation forces, leading to translational movements of the MBs which can push intact MBs into the cell [36]. It could seem that very short pulses (few μs) in combination with high acoustic pressures might be more efficient in terms of drug delivery, but the majority of drug delivery studies still apply long pulses of ms to s [26]. As mentioned in section 2.8, De Cock et al. observed a phenomenon they termed sonoprinting [37]. This was seen after ultrasound treatments using a pulse length of 1000 cycles, a PRF of 100 Hz, with a 1 MHz center frequency and an MI of 0.3, for a total duration of 5 s.

While the two former studies referred to here study uptake of single molecules such as propidium iodine (PI) or green fluorescent protein (GFP), De Cock et al. uses MBs loaded with polystyrene nanospheres on their surface. This approach more resembles the one used in this thesis, and the results from De Cock's paper is one of the reasons why this thesis exists. It was therefore appropriate to try to replicate their results, and compare their approach with what has been used up until this point. To achieve this, two different duty cycles and two different MIs were used on the same CLINIcell, as described in section 4.1.3. One of the four treatments were thus a replica of De Cock's treatment, the only difference being exposure duration, which was kept at 1 min to avoid having too many variables. In any case, it was believed that increasing the duration from 5 s to 1 min would not eliminate the effect seen in De Cock's study.

As mentioned in the beginning of this section, several studies report seing an effect of varying the pulse length and/or the PRF. Indeed, Qui et al. concluded that increasing the PRF had the same effect on cell morphology as increasing the MI, leading to larger membrane pores [44]. Though, as we have seen several times already in this report, the NP-stabilized MBs do not necessarily behave

like the bubbles used in other studies. Figure 21a shows that increasing the PRF does lead to a significantly higher uptake. However, this observation is not clearly reflected in the representation of each individual trial (figures 20a and 20b) and thus it might prove to be premature to make any conclusion from these data. It in unclear why there is such a big difference between the two identical trials shown in figure 20a and figure 20b, specifically the 0.3 MI/50 Hz and 0.59 MI/100 Hz treatments. It is possible that, by chance, very few successfully sonoporated cells were imaged in these two treatment areas in the first trial.

The amount of NPs colocalized with cell membranes increases significantly with increasing PRF (figure 21b). Applying a frequency of 100 Hz leads to about 8 times more colocalized pixels than when using 50 Hz. This could be an effect of the increased radiaton force associated with increasing pulse length and PRF [51, 36], which would push MBs, as well as NP aggregates, against cell membranes, promoting adhesion of these bubbles, or aggregates, to the membrane. Additionally, it seems from figure 22 that increasing the duty cycle increases the amount of aggregation due to secondary Bjerknes forces, leading to larger aggregates. As larger aggreagates will be more heavily affected by radiation forces, this could further increase the amount of particles attached to cell membranes.

The aggregates formed when using high duty cycles and the ones using MIs of 0.1 and 0.2 do not look identical (figures 19 and 22), and their location in particular is an important aspect. While the aggregates from the high duty cycle treatment seems to be closesly associated with cell membranes, the aggregates in the low MI experiments seems to be independent of the cells and more randomly located in the sample. This is supported by comparing the amount of colocalized NPs for the two experiments, which shows more than twice as much NPs associated with cell membranes using an increased duty cycle as compared to lowering the MI (figure 21d).

Comparing the different MIs at the high duty cycle setting shows a significant increase in colocalized NPs for the lowest MI (figure 21c). As previously discussed, increasing the MI will lead to smaller shell fragments after bubble collapse [46]. As larger particles are more strongly influenced by radiation forces than smaller particles [35], lowering the MI might promote the effect of NP aggregates being pushed towards and being embedded into the cell membranes. However, as discussed already, it seems more likely that the NP shell of our MBs do not break up in the same way as lipid MBs, and thus, the aggregates must be formed by free NPs. Nevertheless, it is possible that there are larger particles formed by the lower MI than the higher MI, in combination with a high PRF and pulse length.

Part of the reason for looking at these exact settings was to replicate the results of sonoprinting seen by De Cock [37]. Indeed, by increasing the PRF and cycle length to match that of De Cock, much more NPs was seen colocalized to cell membranes. The elongated shape of the patches of NPs deposited onto cell membranes seen here very much resembles the results seen in De Cock's

paper. In their paper, however, they saw an increase in uptake only during flow cytometry after the observed sonoprinting had taken place, and not during or immediately after treatement. Since the cells in this thesis are only imaged and analysed once, it is impossible to say whether the deposited NPs are ingested by the cells after imaging. However, from figure 20, there is no trend of increasing uptake from the first to the last treatment, which involves a time span during imaging of a few hours. It therefore seems that the deposited NPs are not ingested by the cells. Furthermore, the cell in figure 24 does not seem to ingest a significant amount of the NPs, initially colocalized with its cell membrane, over time, further supporting this point. It must be noted however that the experiment of figure 24 was performed at 4°C with lower PRF and pulse length than the sonoprinting conditions. It should not be ruled out that the high duty cycle could be necessary to elicit sonoprinting.

If the observed NP deposition seen in figure 22 is infact sonoprinting, the lack of uptake following deposition of NP patches, might once again be explained by the different MBs used. Although De Cock et al. used MBs loaded with NPs, the MBs themselves have a lipid shell, which, as discussed, might come with a higher degree of flexibility and responsiveness to the ultrasound treatment than our NP-stabilized MBs. The process of lipid shell fragmentation is called lipid shedding, and has been detected in multiple studies [52, 53]. De Cock et al. hypothesize that the lipid shell fragments carry the NPs to the cell membrane after shedding, and that the uptake mechanism following this is a form of fusion of the lipid fragments and the lipid cell membrane. Although there is presedence for polymer shells to undergo a similar sort of shedding process [54], the polymer fragments would not be able to fuse with the membrane in the same way.

The increase in uptake after ultrasound treatment seen by De Cock et al. is much higher than what is seen here [37], which also supports the hypothesis that sonoprinting was not involved as an uptake mechanism in the present study. Alternatively, using NP-stabilized MBs instead of lipid MBs could lead to a very slow version of sonoprinting uptake. Instead of lipid fusion with the plasma membrane, the deposited pieces of the MB shell could be ingested through endocytosis, which would likely happen less rapidly than lipid fusion. Therefore, *if* sonoprinting-based uptake is taking place in the present study, it will not lead to a significantly more efficient uptake of PIHCA NPs.

Even if the sonoprinting uptake mechanism reported by De Cock et al. was not observed in this experiment, increased uptake, compared to untreated cells, was seen when applying the higher duty cycle. As the treatment causes a lot of NP aggregation, it must be considered that the problem of false uptake because of limitations of the analysis tool, described in section 5.1, is still present to some extent here. Assuming that an increased uptake compared to the control would still be seen if adjusting for this false uptake, a likely explanation to this increase is sonoporation. If sonoporation is achieved using the lower duty cycle, there is no apparent reason why it should not also occur with these new settings, increasing the PRF. If anything the pores could even be bigger [44]. Indeed, De Cock et al. observed pore formation in cells alongside sonoprinting. The

two phenomena was however not colocalized, from which they concluded that sonoporation was not the only, or dominant, mechanism [37]. Considering the vast amount of free NPs in the CLINIcell during treatment, it is possible that these NPs can rush in through such pores, leading to the observed uptake. As mentioned however, it is likely the NPs of the MB shell, and not the free NPs, which enter cells during treatment. Rather than the shell NPs being printed onto the cell membrane, and free NPs being taken up, it therefore seems more probable that the shell NPs are taken up, while free NPs aggregate and deposit onto cell membranes.

5.4 Co-incubation of free NPs and MBs

The unique aspect of this thesis is the type of MBs used. In most of the papers referred to in this discussion, commercial MBs are used, such as Sonovue [34], Targestar [51, 43], Definity [45] or Optison [45], to name a few. These commercial MBs usually have a shell made of lipids, polymers or proteins [55]. The use of such well-known MBs provides predictability, which can be valuable in studies like these. However, the use of these MBs are usually aimed at enhancing uptake of small molecules like dextrans [42, 34], PI [43] or calcein [50], with sizes ranging from a few to tens of nanometers. These commercial MBs might not work in combination with for example NPs, which are usually much bigger than this. De Cock et al. used a MB with NPs attached to the surface via a linker molecule [37] when they observed sonoprinting. To the best of our knowledge, MBs stabilized by a shell of NPs has not been used before. It is therefore key to see how these MBs compare to commercial MBs in enhancing uptake of PIHCA NPs.

Comparing co-incubation of free NPs and Sonazoid MBs with the use of NP-stabilized MBs (figures 27 and 28), shows that the NP-stabilized MBs are significantly more effective at enhancing drug delivery than commercial Sonazoid MBs. This means either that the Sonazoid MBs creates a weaker biophysical effect in the cells, or that the free NPs are not sufficiently close to the pores created, and thus can not enter the cells through them.

Sonazoid MBs are made up of a monomolecular membrane of hydrogenated egg phosphatidyl serine (HEPS) [56], which is a type of lipid membrane. As Sonazoid is relatively recently approved as a contrast agent - only approved in Japan and Korea as of late 2012 [55] - there is not as much research involving this MB as for example Sonovue. It does however seem reasonable to assume that the behaviour of Sonazoid MBs is comparable to other commercially available lipid-shelled MBs, including the response to different acoustic pressures. If so, the pressures used in this experiment should be suitable to result in inertial cavitation and subsequent collapse of the MBs. MIs of 0.32 to 0.85 were used and, according to Bouakaz, MIs above 0.3 can lead to destruction of MBs [28]. As they used MBs with a harder shell than Sonazoid, it seems probable that the MIs used in this thesis would result in inertial caviation of Sonazoid MBs.

Even if the applied MIs were suitable, the Sonazoid MBs will possibly respond differently to the applied ultrasound than the NP-stabilized MBs. Al-

though it seems that the two MB types are comparable in their response to ultrasound, as discussed above, it is possible that the collapse of the two MBs differ. Due to the different compositions of the two shells, it can not ruled out that the NP-stabilized MB collapses in a more violent manner, leading to larger pores. It is therefore possible that the flexibility of the lipid shell of the Sonazoid MBs puts a limit on the size of the pores these MBs can create, a limit which is below the size of the NPs used in this project (average size of 177 nm). Pore sizes of up to several μm have been reported for phospholipid-based MBs [57], but this was with ultrasound of 1.3 MHz (compared to our 1 MHz) and MI 1.2, which is substantially higher than the maximum MI of 0.85 used here. However, since it was concluded that stable cavitation of the NP-stabilized MBs also plays a role in the uptake, it seems more likely that the explanation to the lack of uptake when using Sonazoid has to do with the absence of NPs on its surface.

The NP shell, or rather the presence of NPs at the MB surface is a crucial part of the design of the NP-stabilized MBs. The design is based on the desire to have NPs localized at the MBs to ensure close proximity between the NPs and the pore openings. The pores created by sonoporation are transient and close fast, usually within a few seconds, and no more than a couple of minutes [26, 58]. This means that if the NPs are not present at the pore openings immediately after they occur, they might not be taken up into the cell.

Based on the surface area of an average NP-stabilized MB (d=2.5 μm) and the cross-sectional area of a NP (d=177 nm), and rounding up to account for an imperfect shell (not an exact thickness of one NP around the whole MB) one can estimate that there is about 1000 NPs in each MB shell (confirmed by personal communication with the manufacturer). Considering that only 1% of the NPs in the MB solution is actually part of MB shells, this gives around $5 \cdot 10^{13}$ NPs per mL MB solution. When co-incubating free NPs with commercial MBs the same amount of NP is used. This is an extremely high number, which makes it unlikely that the distance between NPs and pores should be an issue. With a number such as this, the NPs should be virtually everywhere. Yet, as stated, the cavitation of the MBs themselves pushed these free NPs away. It is possible that the increased uptake compared to the control seen using Sonazoid MBs is a result of some entry of free NPs through pores. If so, it is likely that this also happens when using NP-stabilized MBs. Possibly, there will always be some entry of free NPs, but it is the shell NPs of hte NP-stabilized MBs that makes the difference so large. The increase in uptake seen with Sonazoid MBs could also be a result of enhanced endocytosis.

5.5 Future work and clinical applications

For sonoporation to be a reliable alternative for future cancer treatment, a deeper understanding of the process needs to be gained. One useful approach is to use monodisperse MBs to study how the size of MBs affect the resulting biophysical reactions in the cells. It is known that the size of the MBs does matter [28], but the dependency of the size might vary between different types

of MBs depending of other factors, such as MB shell composition or the kind of MB core. In this thesis the MBs had an average diameter of around 2.5 μm, but with a large degree of polydispersity. Because of this it becomes impossible to say anything about how the MB size affected the results. The fact that clustered uptake was not seen to a greater extent could indicate that the ideal MB size lies far below or above the average diameter for the MBs used, and thus only a few MBs responded in a desired way. If one could use monodisperse MBs however, this size dependency could be uncovered, which would be a very useful tool. The obvious challenge is the manufacturing of monodisperse MBs. Because the current MBs are made by stirring air into a solution containing NPs, there is very little control over MB size. One possible way of obtaining monodisperse MBs is by using microfluidics. However the monodispersity is achieved, it could prove decisive for the relevance of sonoporation in the future.

Another parameter that should be considered is the effect of varying the size of the NPs used. By using smaller or bigger NPs than the ones used in this project, important insight could be gained into the effect of sonoporation, both in terms of effect on the cells, and uptake mechanisms of NPs. By using a certain MI and a certain ultrasound setting, but varying the size of the NPs, it should be possible to eventually establish how big pores the treatment causes. This is important in order to find the optimal ultrasound treatment for a particular use - the optimal being the treatment which causes the least damage to tissue but still gets the NPs into the cells. Another interesting point would be to use differently sized NPs for different cavitation modes. Potentially one could see NPs of a certain size being taken up after intertial cavitation but not after stable cavitation, and by varying NP sizes, the different size limits could be established.

Another consideration of interest is how the effect of the ultrasound treatment varies between different cell lines. Ideally, if sonoporation was to succeed in cancer treatment, it would have to be applicable to more types of cancer than prostate cancer. It is therefore important to study how the effect of sonoporation, using PIHCA stabilized MBs, varies between cell lines. Will the amount of uptake in a given cell line after ultrasound treatment correlate with the cell lines natural predisposition to endocytose the NPs in the absence of ultrasound? Or will perhaps sonoporation not work on all cell lines? These are important questions to answer, the answers to which will directly impact the potential usefulness of sonoporation. Some research has been done on the uptake of PACA NPs (specifically PBCA and POCA) in different cell lines [13], but not with PIHCA NPs. The effect of sonoporation with NP-stabilized MBs on different cell lines, as well as the effect of varying the NP size, was intended to be explored in this thesis. Unfortunately, due to problems with the treatment setup during these experiments, the results could not be used.

All of these aspects concern the basic understanding of how sonoporation works, and how it can and should be used in combination with NP-stabilized MBs. Understanding these principles is key in the evolution of sonoporation as a medical tool. Many of the questions regarding sonoporation could be answered

if one could look at a MB in contact with a cell while it was being exposed to ultrasound. This is possible if one has a setup that allows for simultaneous treatment and imaging. Such a setup exists at St. Olavs Hospital in Trondheim, and live investigations of MB behaviour would be an exciting next step in learning about sonoporation.

Finally, the effect of fixation of cells should be studied. The fact that cellular uptake, in some form, was seen in every single experiment during this thesis, as compared to the project thesis where fixation was used, proves that chemical fixation impares cellular uptake. How this imparement works however, remains unclear. It would be interesting to treat the cells like they have been in this experiment, but using real-time microscopy, and establishing successful sonoporation before adding the fixation chemicals. That way one could observe a successfully sonoporated cell as fixation is taking place, in order to study how fixation removes the visible uptake.

Sonoporation is indeed an exciting possibility to improve and enhance cancer treatment in the future. Considering the positive results using NP-stabilized MBs in this thesis, it is easy to be optimistic with respect to its potential clinical use. It is important to remember the biological limitations that makes sonoporation difficult for real life treatment: The MBs are too large to escape from the blood vessel. Although some approaches to solving this exists, including nanoemulsions, a MB stabilized by a shell of NPs seems to be impossible to get into the tumor without direct injection into the tumor tissue. Even so, some applications of sonoporation using this type of MB do exist. Dewitte et al. recently used sonoporation of dendritic cells for immunotherapy experiments, with promising results [38]. By extracting cells from the animals, sonoporation could be performed in vitro, before the cells were injected into the animals again. This is one example of a promising applications of sonoporation, and many more could emerge in the years to come.

6 Conclusion

Two forms of cellular uptake was observed after ultrasound treatment. It is hypothesized that clustered uptake is a result of sonoporation, while simple uptake is a result of normal endocytosis. It can however not be ruled out that enhanced endocytosis might also contribute to cellular uptake with the appearance of simple uptake, as enhanced and normal endocytosis can be hard to separate, at least qualitatively.

Applying an MI of 0.1 did not lead to a significant increase in uptake compared to untreated control cells. While increasing the MI from 0.1 to 0.2 lead to a significant increase in cellular uptake, any increase in acoustic pressure above 0.2 did not lead to a corresponding increase in cellular uptake.

Because a response of the MBs was seen at an MI of 0.2, the behaviour of the MBs seem to resemble flexible lipid MBs, rather than hard-shelled MBs as first believed. It therefore seems likely that stable cavitation of the MBs lead to membrane disruptions, or pores, through which NPs from the MB shell can enter the cell. As the MI increases, the cavitation mode will at some point go from stable to inertial, but this does not seem to greatly affect the cellular uptake of PIHCA NPs.

The observation that 0.1 MI does not lead to significantly increased uptake leads to the conclusion that there exists an acoustic pressure threshold, below which the cavitation of the MBs does not lead to large enough pores in the cell membranes for the NPs to enter. Above this threshold, the pores seems to be large enough for entry of the same amount of NPs, regardless of MI. It is hypothesized that these observations can be explained by the composition of the MB. As the MB shell consists of individual NPs, it seems that the shell breaks up into rather small pieces, the sizes of which are largely independent of the applied MI, as opposed to lipid shedding which results in broken off patches of the MB shell.

Additionally, because the NPs of the MB shell are taken up, rather than the free NPs in the solution, which are pushed away by the cavitation of the MBs, the same amount of NPs are available for uptake in each sonoporation event. This amount corresponds to the amount of NPs that make up a MB.

Ultrasound treatment at 4°C also resulted in significantly increased uptake compared to the control, and the amount of uptake was comparable to the similar experiment performed at 37°C. This rules out enhanced endocytosis as a major uptake mechanism, as this would not occur at 4°C, and supports the theory that uptake happens through sonoporation. A trend of increasing uptake was seen, owing to the increasing temperature and thus increasing amount of normal endocytosis during imaging.

Increasing the pulse length and PRF to 1000 and 100 Hz, respectively, lead to a significant increase in uptake compared to 100 cycles and 50 Hz PRF, although no definitive conclusions should be made here considering the variations between the two trials. Furthermore, the increased duty cycle lead to a large increase in the amount of colocalized NPs. This colocalization is not believed to be a result of sonoprinting however, as it seems more probable that the NPs of the

MB shell are taken up by the cell, while it is the free NPs that aggregate and deposit onto cell membranes.

Co-injection of commercial Sonazoid MBs also lead to an increased uptake compared to untreated cells, but the uptake was significantly lower than when using PIHCA-stabilized MBs. It seems that the presence of NPs on the MB surface is crucial for sonoporation to be successful. The modest increase in uptake observed using Sonazoid MBs might be due to some free NPs rushing into the cell through an open pore, or due to enhanced endocytosis. In either case this shows that neither uptake of free NPs nor enhanced endocytosis plays a major role in the cellular uptake of PIHCA NPs.

In conclusion, successful uptake of NPs through sonoporation was achieved in this project. Although the uptake, compared to untreated control cells, was significantly increased, this increase might be far too low for sonoporation using PIHCA-NP stabilized MBs to be used in a clinical setting. This seems to be mainly attributed to the relatively low occurence of clustered uptake, indicating successfully sonoporated cells. Real-time microscopy investigations of the behaviour of these MBs during ultrasound treatment will reveal important characteristics, the understanding of which can prove vital for increasing the success rate of sonoporation. If the sonoporation process was to be fully understood and controlled, the uptake could increase several folds compared to what was achieved in this project.

References

[1] B. Stewart and C. P. Wild, "World Cancer Report 2014," *International Agency for Research on Cancer, WHO*, 2014.

[2] J. Hardin, G. Bertoni, and L. J. Kleinsmith, *Beckers's World of the Cell*. Pearson, eighth edi ed., 2012.

[3] K. Cho, X. Wang, S. Nie, Z. Chen, and D. M. Shin, "Therapeutic nanoparticles for drug delivery in cancer," *Clinical Cancer Research*, vol. 14, no. 5, pp. 1310–1316, 2008.

[4] J. V. Jokerst, T. Lobovkina, R. N. Zare, and S. S. Gambhir, "Nanoparticle PEGylation for imaging and therapy," *Nanomedicine (Lond)*, vol. 6, no. 4, pp. 715–728, 2011.

[5] G. Storm, S. O. Belliot, T. Daemen, and D. D. Lasic, "Surface modification of nanoparticles to oppose uptake by the mononuclear phagocyte system," *Advanced Drug Delivery Reviews*, vol. 17, no. 1, pp. 31–48, 1995.

[6] Ý. Mørch, R. Hansen, S. Berg, A. K. O. Åslund, W. R. Glomm, S. Eggen, R. Schmid, H. Johnsen, S. Kubowicz, S. Snipstad, E. Sulheim, S. Hak, G. Singh, B. H. McDonagh, H. Blom, C. de Lange Davies, and P. M. Stenstad, "Nanoparticle-stabilized microbubbles for multimodal imaging and drug delivery," *Contrast Media & Molecular Imaging*, no. August 2014, pp. n/a–n/a, 2015.

[7] American Cancer Society, "Cancer Treatment & Survivorship Facts and Figures 2014-2015," *Atlanta: American Cancer Society*, p. 44, 2014.

[8] K. H. Bae, H. J. Chung, and T. G. Park, "Nanomaterials for cancer therapy and imaging," *Molecules and Cells*, vol. 31, no. 4, pp. 295–302, 2011.

[9] Y. Matsumura and H. Maeda, "A New Concept for Macromolecular Therapeutics in Cancer Chemotherapy: Mechanism of Tumoritropic Accumulation of Proteins and the Antitumor Agent Smancs," *Cancer Research*, vol. 46, no. 8, pp. 6387–6392, 1986.

[10] S. Torosean, B. Flynn, J. Axelsson, J. Gunn, K. S. Samkoe, T. Hasan, M. M. Doyley, and B. W. Pogue, "Nanoparticle uptake in tumors is mediated by the interplay of vascular and collagen density with interstitial pressure," *Nanomedicine: Nanotechnology, Biology, and Medicine*, vol. 9, no. 2, pp. 151–158, 2013.

[11] A. K. Iyer, G. Khaled, J. Fang, and H. Maeda, "Exploiting the enhanced permeability and retention effect for tumor targeting," *Drug Discovery Today*, vol. 11, no. 17-18, pp. 812–818, 2006.

[12] D. Peer, J. M. Karp, S. Hong, O. C. Farokhzad, R. Margalit, and R. Langer, "Nanocarriers as an emerging platform for cancer therapy.," *Nature nanotechnology*, vol. 2, no. 12, pp. 751–760, 2007.

[13] E. Sulheim, H. Baghirov, E. von Haartman, A. Bøe, A. K. O. Åslund, Y. Mørch, and C. d. L. Davies, "Cellular uptake and intracellular degradation of poly(alkyl cyanoacrylate) nanoparticles.," *Journal of nanobiotechnology*, vol. 14, no. 1, p. 1, 2016.

[14] S. Stolnik, L. Illum, and S. S. Davis, "Long circulating microparticulate drug carriers," *Advanced Drug Delivery Reviews*, vol. 64, no. SUPPL., pp. 290–301, 2012.

[15] V. Frenkel, "Ultrasound mediated delivery of drugs and genes to solid tumors," *Advanced Drug Delivery Reviews*, vol. 60, no. 10, pp. 1193–1208, 2008.

[16] H. Hillaireau and P. Couvreur, "Nanocarriers' entry into the cell: Relevance to drug delivery," *Cellular and Molecular Life Sciences*, vol. 66, no. 17, pp. 2873–2896, 2009.

[17] C. He, Y. Hu, L. Yin, C. Tang, and C. Yin, "Effects of particle size and surface charge on cellular uptake and biodistribution of polymeric nanoparticles," *Biomaterials*, vol. 31, no. 13, pp. 3657–3666, 2010.

[18] T. dos Santos, J. Varela, I. Lynch, A. Salvati, and K. A. Dawson, "Effects of transport inhibitors on the cellular uptake of carboxylated polystyrene nanoparticles in different cell lines.," *PloS one*, vol. 6, no. 9, p. e24438, 2011.

[19] G. A. Husseini, W. G. Pitt, and A. M. Martins, "Ultrasonically triggered drug delivery: Breaking the barrier," *Colloids and Surfaces B: Biointerfaces*, vol. 123, pp. 364–386, 2014.

[20] W. D. O'Brien, "Ultrasound-biophysics mechanisms," *Progress in Biophysics and Molecular Biology*, vol. 93, no. 1-3, pp. 212–255, 2007.

[21] A. Schroeder, J. Kost, and Y. Barenholz, "Ultrasound, liposomes, and drug delivery: principles for using ultrasound to control the release of drugs from liposomes," *Chemistry and Physics of Lipids*, vol. 162, no. 1-2, pp. 1–16, 2009.

[22] R. E. Apfel and C. K. Holland, "Gauging the likelihood of cavitation from short-pulse, low-duty cycle diagnostic ultrasound," *Ultrasound in Medicine and Biology*, vol. 17, no. 2, pp. 179–185, 1991.

[23] J. Wu and W. L. Nyborg, "Ultrasound, cavitation bubbles and their interaction with cells," *Advanced Drug Delivery Reviews*, vol. 60, no. 10, pp. 1103–1116, 2008.

[24] A. Burgess and K. Hynynen, "Noninvasive and targeted drug delivery to the brain using focused ultrasound," *ACS chemical neuroscience*, vol. 4, no. 4, pp. 519–526, 2013.

[25] B. Y. J. Lee Hak Jong Yoon Young Il, "Theragnostic ultrasound using microbubbles in the treatment of prostate cancer," *Ultrasonography*, vol. 0, no. 0, p. 0, 2016.

[26] I. Lentacker, I. De Cock, R. Deckers, S. C. De Smedt, and C. T. W. Moonen, "Understanding ultrasound induced sonoporation: Definitions and underlying mechanisms," *Advanced Drug Delivery Reviews*, vol. 72, pp. 49–64, 2014.

[27] S. H. Bloch, M. Wan, P. A. Dayton, and K. W. Ferrara, "Optical observation of lipid- and polymer-shelled ultrasound microbubble contrast agents," *Applied Physics Letters*, vol. 84, no. 4, pp. 631–633, 2004.

[28] A. Bouakaz, M. Versluis, and N. de Jong, "High-speed optical observations of contrast agent destruction," *Ultrasound in Medicine & Biology*, vol. 31, pp. 391–399, mar 2005.

[29] K. Kooiman, H. J. Vos, M. Versluis, and N. De Jong, "Acoustic behavior of microbubbles and implications for drug delivery," 2014.

[30] D. O. Draper, J. C. Castel, and D. Castel, "Rate of temperature increase in human muscle during 1 MHz and 3 MHz continuous ultrasound.," *The Journal of orthopaedic and sports physical therapy*, vol. 22, no. 4, pp. 142–50, 1995.

[31] W. G. Pitt, G. A. Husseini, and B. J. Staples, "Ultrasonic drug delivery–a general review.," *Expert opinion on drug delivery*, vol. 1, no. 1, pp. 37–56, 2004.

[32] R. Deckers and C. T. W. Moonen, "Ultrasound triggered, image guided, local drug delivery," *Journal of Controlled Release*, vol. 148, no. 1, pp. 25–33, 2010.

[33] A. A. Doinikov, *Bubble and particle dynamics in acoustic fields : modern trends and applications*. Research Signpost, 2005.

[34] B. D. M. Meijering, L. J. M. Juffermans, A. Van Wamel, R. H. Henning, I. S. Zuhorn, M. Emmer, A. M. G. Versteilen, W. J. Paulus, W. H. Van Gilst, K. Kooiman, N. De Jong, R. J. P. Musters, L. E. Deelman, and O. Kamp, "Ultrasound and microbubble-targeted delivery of macromolecules is regulated by induction of endocytosis and pore formation," *Circulation Research*, vol. 104, no. 5, pp. 679–687, 2009.

[35] P. Qin, L. Jin, Fan Li, Tao Han, L. Du, and A. C. H. Yu, "The relationship between microbubble size and heterogeneous sonoporation at the single-cell level," *2016 IEEE International Ultrasonics Symposium (IUS)*, pp. 1–4, 2016.

[36] Y. Zhou, K. Yang, J. Cui, J. Y. Ye, and C. X. Deng, "Controlled permeation of cell membrane by single bubble acoustic cavitation," *Journal of Controlled Release*, vol. 157, no. 1, pp. 103–111, 2012.

[37] I. De Cock, G. Lajoinie, M. Versluis, S. C. De Smedt, and I. Lentacker, "Sonoprinting and the importance of microbubble loading for the ultrasound mediated cellular delivery of nanoparticles," *Biomaterials*, vol. 83, pp. 294–307, 2016.

[38] H. Dewitte, S. Van Lint, C. Heirman, K. Thielemans, S. C. De Smedt, K. Breckpot, and I. Lentacker, "The potential of antigen and TriMix sonoporation using mRNA-loaded microbubbles for ultrasound-triggered cancer immunotherapy," *Journal of Controlled Release*, vol. 194, no. 1, pp. 28–36, 2014.

[39] M. D. DB. Murphy, "Confocal Laser Scanning Microscopy," *Fundamentals of Light Microscopy and Electronic Imaging*, pp. 265–305, 2012.

[40] S. W. Paddock, "Principles and practices of laser scanning confocal microscopy.," *Molecular biotechnology*, vol. 16, no. 2, pp. 127–149, 2000.

[41] Mabio, "Specifications of CLINIcell cell culture system."

[42] M. Afadzi, S. Strand, E. A. Nilssen, S. E. Masoy, T. Johansen, R. Hansen, B. Angelsen, and C. De L. Davies, "Mechanisms of the ultrasound-mediated intracellular delivery of liposomes and dextrans," *IEEE Transactions on Ultrasonics, Ferroelectrics, and Frequency Control*, vol. 60, no. 1, pp. 21–33, 2013.

[43] Z. Fan, H. Liu, M. Mayer, and C. X. Deng, "Spatiotemporally controlled single cell sonoporation.," *Proceedings of the National Academy of Sciences of the United States of America*, vol. 109, pp. 16486–91, oct 2012.

[44] Y. Qiu, Y. Luo, Y. Zhang, W. Cui, D. Zhang, J. Wu, J. Zhang, and J. Tu, "The correlation between acoustic cavitation and sonoporation involved in ultrasound-mediated DNA transfection with polyethylenimine (PEI) in vitro," *Journal of Controlled Release*, vol. 145, pp. 40–48, jul 2010.

[45] R. Karshafian, S. Samac, P. D. Bevan, and P. N. Burns, "Microbubble mediated sonoporation of cells in suspension: Clonogenic viability and influence of molecular size on uptake," *Ultrasonics*, vol. 50, pp. 691–697, jun 2010.

[46] S. Ibsen, G. Shi, C. Schutt, L. Shi, K. D. Suico, M. Benchimol, V. Serra, D. Simberg, M. Berns, and S. Esener, "The behavior of lipid debris left on cell surfaces from microbubble based ultrasound molecular imaging," *Ultrasonics*, vol. 54, no. 8, pp. 2090–2098, 2014.

[47] V. Idone, C. Tam, J. W. Goss, D. Toomre, M. Pypaert, and N. W. Andrews, "Repair of injured plasma membrane by rapid Ca2+ dependent endocytosis," *Journal of Cell Biology*, vol. 180, no. 5, pp. 905–914, 2008.

[48] H. Medwin, "Acoustical determinations of bubble-size spectra," *The Journal of the Acoustical Society of America*, vol. 62, no. 4, p. 1041, 1977.

[49] J. Hauser, M. Ellisman, H.-U. Steinau, E. Stefan, M. Dudda, and M. Hauser, "ULTRASOUND ENHANCED ENDOCYTOTIC ACTIVITY OF HUMAN FIBROBLASTS," *Ultrasound in Medicine & Biology*, vol. 35, pp. 2084–2092, 2009.

[50] X. Chen, Y. Hu, R. Leow, A. Yu, and J. Wan, "How sonoporation disrupts cellular structural integrity: morphological and cytoskeletal observations," 2013.

[51] Z. Fan, D. Chen, and C. X. Deng, "Improving ultrasound gene transfection efficiency by controlling ultrasound excitation of microbubbles," *Journal of Controlled Release*, vol. 170, no. 3, pp. 401–413, 2013.

[52] Y. Luan, G. Lajoinie, E. Gelderblom, I. Skachkov, A. F. W. Van Der Steen, H. J. Vos, M. Versluis, and N. De Jong, "LIPID SHEDDING FROM SINGLE OSCILLATING MICROBUBBLES," *World Federation for Ultrasound in Medicine & Biology*, 2014.

[53] M. A. Borden, D. E. Kruse, C. F. Caskey, S. Zhao, P. A. Dayton, and K. W. Ferrara, "Influence of lipid shell physicochemical properties on ultrasound-induced microbubble destruction," *IEEE Transactions on Ultrasonics, Ferroelectrics, and Frequency Control*, vol. 52, no. 11, pp. 1992–2002, 2005.

[54] J. R. Eisenbrey, M. C. Soulen, and M. A. Wheatley, "Delivery of encapsulated doxorubicin by ultrasound-mediated size reduction of drug-loaded polymer contrast agents," *IEEE Transactions on Biomedical Engineering*, vol. 57, no. 1, pp. 24–28, 2010.

[55] J. Castle, M. Butts, A. Healey, K. Kent, M. Marino, and S. B. Feinstein, "Ultrasound-mediated targeted drug delivery: recent success and remaining challenges," *AJP: Heart and Circulatory Physiology*, vol. 304, no. 3, pp. H350–H357, 2013.

[56] P. Christian Sontum, "PHYSICOCHEMICAL CHARACTERISTICS OF SONAZOID^{TM}, A NEW CONTRAST AGENT FOR ULTRASOUND IMAGING,"

[57] Y.-Z. Zhao, Y.-K. Luo, C.-T. Lu, J.-F. Xu, J. Tang, M. Zhang, Y. Zhang, and H.-D. Liang, "Phospholipids-based microbubbles sonoporation pore size and reseal of cell membrane cultured in vitro.," *Journal of drug targeting*, vol. 16, no. January, pp. 18–25, 2008.

[58] Y. Zhou, J. Shi, J. Cui, and C. X. Deng, "Effects of extracellular calcium on cell membrane resealing in sonoporation," *Journal of Controlled Release*, vol. 126, no. 1, pp. 34–43, 2008.